

Submitted to The Astrophysical Journal

Testing Models of Radio Galaxy Evolution and the Cosmological Impact of FR II Radio Galaxies

Paramita Barai¹, Paul J. Wiita

Department of Physics & Astronomy, Georgia State University, P. O. Box 4106, Atlanta, GA 30302-4106, USA

`pabar56@phy.ulaval.ca, wiita@chara.gsu.edu`

ABSTRACT

We investigate aspects of the cosmological evolution of FR II radio galaxies, focusing first on the abilities of models to match data for linear-sizes, radio powers, redshifts and spectral indices. Here we consider modifications to the theoretical models we had treated earlier, primarily by accounting for the growth of the radius of hotspots with source size. Better fits to the distributions of most of the data in three low-frequency surveys can be found with sensible choices of model parameters but no model yet considered gives a good match to all of the survey data simultaneously, nor does any do a good job of producing the spectral index distributions. The observational datasets are too small to completely discriminate among the models. We calculate the volume fraction of the “relevant universe” cumulatively occupied by the expanding radio galaxy lobes over the quasar era, when these powerful radio galaxies were much more common, and when they have been argued to play an important role in triggering galaxy formation and spreading magnetic fields and metals. We found the cumulative relevant volume filling factor of radio galaxies to be $\sim 5\%$, so we conclude that these impacts are smaller than previously estimated but that they are still significant.

Subject headings: galaxies: active — galaxies: luminosity function, mass function — large-scale structure of universe — methods: statistical — radio continuum: galaxies — surveys

¹current address: Département de physique, de génie physique et d’optique, Université Laval, Québec, QC G1K 7P4, Canada.

1. Introduction

Classical double radio galaxies (RGs) with extended lobes, or the Fanaroff-Riley Class II (FR II) sources, constitute the more powerful RG population. The *quasar era* (i.e., between redshifts $\simeq 1.5$ and 3) is distinguishable by rises in the comoving luminosity densities of RGs, quasars and other powerful AGN (Dunlop & Peacock 1990; Jackson & Wall 1999; Willott et al. 2001; Ueda et al. 2003; Grimes et al. 2004; Hopkins et al. 2006), as well as high star and galaxy formation rates (e.g., Lilly et al. 1996; Madau et al. 1998; Bouwens & Illingworth 2006; Sawicki & Thompson 2006a,b). These similar evolutions suggest that powerful RGs can have substantial impacts on the formation, distribution and evolution of galaxies and large scale structures of the universe (e.g., Gopal-Krishna & Wiita 2001, GKW01; Kronberg et al. 2001; Gopal-Krishna & Wiita 2003a, GKW03a; Gopal-Krishna & Wiita 2003b, GKW03b; Gopal-Krishna, Wiita, & Osterman 2003, GKWO; Gopal-Krishna, Wiita, & Barai 2004, GKWB04; Rawlings & Jarvis 2004; Levine & Gnedin 2005; Silk 2005). Observational investigations show remarkable radio-optical alignment in high- z RGs (e.g., McCarthy et al. 1987; Chambers et al. 1988a,b; Dey et al. 1997; Venemans et al. 2004, 2005; Greve et al. 2006; Overzier et al. 2006; Zheng et al. 2006; Ajiki et al. 2006). Some studies attribute this to FR II RGs triggering extensive star formation in a multi-phase intergalactic medium (IGM) (e.g., Begelman & Cioffi 1989; De Young 1989; Rees 1989; Chokshi 1997; GKW01). In addition, the expanding RG lobes could easily have infused significant magnetic fields into the IGM (GKW01, GKWO, GKWB). Similar conclusions were drawn from different lines of argument by Kronberg et al. (2001) and Furlanetto & Loeb (2001). These radio sources born through the quasar era could also have contributed toward metal enhancement of their environments (GKW03b; GKWB04), since observations (e.g., Dietrich et al. 2003; Schaye et al. 2003; Aguirre et al. 2004; Shapley et al. 2004; Pieri et al. 2006; Prochaska et al. 2006; Tripp et al. 2006) require an efficient mechanism for spreading metals widely at early cosmic epochs.

A comprehensive study of the impact of RGs on various events in the cosmological history of the universe requires reliable quantitative estimates of the relevant volume filling fraction of RGs and their active lifetimes. A prerequisite for a more accurate computation of this volume impacted by radio lobes is a good model of the evolution of radio sources, for both individual sources and as a function of redshift. In a recent work Rawlings & Jarvis (2004) agreed that RG lobes will penetrate much of the relevant universe, but they argued that this may often shut off star formation by expelling gas from protoclusters. However, they assume a single phase medium, unlike our picture or that of Rees (1989), so this negative conclusion is not surprising. Many recent observational studies (e.g., Bohringer et al. 1995; Bîrzan et al. 2004; Choi et al. 2004; O'Dea et al. 2004; Reynolds et al. 2005) show depressions in X-ray surface brightness coinciding with radio lobes, cavities and buoyant bubbles in clusters of galaxies; these are clear signatures of the interactions of radio sources with their surrounding

hot intracluster gas on scales of several tens to hundreds of kiloparsecs from the AGN.

Our aim is to probe in more detail the cosmological impact of RGs on the growth of structures. To do so, we must first develop an improved but essentially analytical model for the evolution of FR II RGs as they age individually and as their numbers vary with cosmological epoch. As our first step toward this goal we (Barai & Wiita 2006, BW) compared three fairly sophisticated analytical models for the dynamical and lobe power evolution of FR II RGs, those given by Kaiser, Dennett-Thorpe, & Alexander (1997, KDA), Blundell, Rawlings, & Willott (1999, BRW) and Manolakou & Kirk (2002, MK); the reader should have some familiarity with these papers or see Barai (2006) for more details. The source linear-size evolution in the BRW and MK models essentially follow the KDA prescription. However the models differ in the ways the relativistic particles are injected from the jet to the lobe, and in treatments of loss terms and particle transport. So there are some significant differences in their predictions for observed powers (P) as functions of source size (D) and redshift (z).

The [P – D] evolutionary tracks of model radio sources have been used in KDA, MK, and in Machalski et al. (2004a,b) as the main way to look for consistency between observational data and RG evolution models. The radio sky simulation prescription in Blundell, Rawlings, & Willott (1999, BRW) adds new dimensions to the observed parameter space. Deriving a RG redshift distribution function from the work of Willott et al. (2001) on the radio luminosity function (RLF), BRW prescribed a virtual RG survey technique. This involves generation of a huge initial population of sources over extended cosmic epoch according to pre-defined distribution functions in redshift, jet power, source age, and orientation. These large numbers of sources then evolve through their individual lives where they interact with their environments and undergo energy losses. Only a few simulated sources are detected in the virtual surveys when mathematical flux limits, corresponding to observations, are imposed. We adopted observational samples from the redshift-complete subsamples: 3CRR (Laing, Riley, & Longair 1983), 6CE (Rawlings, Eales, & Lacy 2001) and 7CRS (McGilchrist et al. 1990), of the Cambridge flux-limited radio catalogs; see Table 2 of BW. The models, relevant observations and the multi-dimensional Monte Carlo simulation methodology leading to the virtual surveys are discussed in detail in §§2 – 4 of BW, and given in more detail in Barai (2006). Using the virtual surveys and any radio lobe power evolution model (KDA, BRW or MK), one can get P , D , z , and spectral index, α (with the convention $P_\nu \propto \nu^{-\alpha}$), values for the simulated model radio sources detected in the pseudo-surveys. The distributions of the characteristics of these simulated RGs can then be compared to observational data to test the model. In order to assess the success of a theoretical model, we perform several statistical tests and present the quantified results for the various model fits. In BW, our main conclusion is that none of the heretofore published models provides an adequate description of the data.

As our next major step toward the goal of isolating good RG models, we have varied the radio lobe power evolution models in the present work. We consider modifications to the original models of BRW and MK, by incorporating a variable hotspot size growing with the source age. Here, we perform analogous simulation-based virtual surveys on the modified models, and present the corresponding statistical results. In §2 we describe the models: Modified BRW (MBRW), Modified MK (MMK), K2000 (Kaiser 2000) and the alternative radio luminosity function (RLF). We give the statistical test results of the model simulations in §3, which we discuss in §4.

One important goal of this work has been to address the question of what fraction of the relevant volume of the universe (the volume containing most of the cosmic baryons) did the radio lobes occupy during the quasar era (GKW01). The warm/hot intergalactic medium (WHIM) comprises the main repository of cosmic baryons which can potentially collapse to form star clusters or galaxies (e.g., Cen & Ostriker 1999). So the radio lobes need to penetrate a significant portion of this “relevant volume of the universe” occupied by the WHIM filaments in order to have a significant role in impacting star formation and spreading magnetic fields and metals (e.g., GKWB04; BGKOW04 and references therein). In §5 we calculate the total volume filled by the RGs over the quasar era (when their population peaked) as a fraction of the relevant volume of the universe. Our conclusions are in §6.

2. Modified Radio Galaxy Evolution Models

The major modification to the BRW and MK models involved allowing the hotspots to grow in size as a source ages and expands. The data used to make a sensible modification are taken from Jeyakumar & Saikia (2000, hereafter JS00), who studied the dependence of sizes of hotspots on overall source sizes for a sample of FR II sources which included both compact steep spectrum and larger-sized sources spanning a projected source size range from about 50 pc to nearly 1 Mpc (Fig. 1). We parameterize the hotspot radius,

$$r_{hs} = r_{hs0} + f(L), \quad (1)$$

where r_{hs0} is some normalizing initial hotspot radius, and $f(L)$ is a power law expression of the total linear size L of the source. We chose r_{hs0} such that the hotspot of a source grows to $r_{hs} = 2.5$ kpc when the total linear size is $L = 200$ kpc, since these are reasonable averages of the actual values and $r_{hs} = 2.5$ kpc was the constant value assumed by BRW.

The hotspot and source angular size data are adopted from JS00. We follow these authors and find the average angular hotspot size for each source. This is the geometric mean of each hotspot (major and minor axes) sizes and, for those sources with hotspots

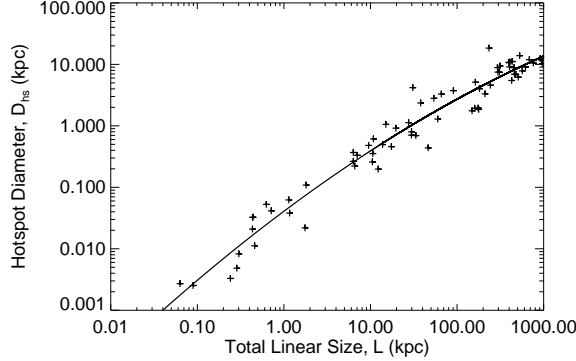


Fig. 1.— Quadratic curve fit to the hotspot size vs. linear size, $[D_{hs}-L]$ data of Jeyakumar & Saikia (2000) (§2).

detected on both sides, the arithmetic average of their sizes. We convert the angular hotspot sizes and separations to corresponding projected linear sizes using the consensus cosmology (Spergel et al. 2006). Total linear sizes (L) are obtained by assuming an average angle to the line of sight of 39.5° (following KDA, as done for the $[P-D]$ tracks in BW §5.1). The hotspots are much smaller than the total source sizes and are assumed to be spherical, so projection effects are negligible for them.

We performed various least-squares fits to the $\log(r_{hs})$ vs. $\log(L)$ data: a single straight line; a single quadratic; two straight lines with a break at 20 kpc; two straight lines with a break at 1 kpc. Although all these fits are satisfactory, a quadratic fit to the data gave the lowest reduced χ^2 and is shown in Fig. 1. So the hotspot size was taken to be growing with the source size as

$$\log(D_{hs}) = c_{hs1} + y_1 \log L + y_2 (\log L)^2. \quad (2)$$

Then the hotspot radius was given by Eq. (1) using $f(L) = D_{hs}/2$. The best fit values of the coefficients are $c_{hs1} = -3.199$, $y_1 = 1.053$, and $y_2 = -0.0306$, which gave a reduced $\chi^2_r = 0.2720$. Perucho & Martí (2003) presented a dynamical model for compact-symmetric and FR II sources where the hotspot size grows self-similarly with linear size, and can get a fit which is in agreement with the results of Jeyakumar & Saikia (2000).

In the modified BRW (MBRW) model the hotspot size (and area, $A_{hs} = \pi r_{hs}^2$) rises according to Eqs. (1) and (2). It otherwise follows the prescription of the original BRW model summarized in §3.3 of BW. During a source’s evolution several additional quantities (which were fixed for a source when a constant hotspot size was assumed) also varied with its age. These include the hotspot pressure, p_{hs} , the hotspot magnetic field, B_{hs} , the “slow” and “fast” break frequencies, ν_{bs} and ν_{bf} , and the corresponding critical Lorentz factors, γ_{bs}

and γ_{bf} .

The modified MK (MMK) model also incorporates the same rising hotspot size (and area). In the MK model, the characteristic time, t_0 , (Eq. 6 of MK) when the size of the head was comparable to the hotspot size, depends on “an initial” hotspot area $A_{hs(t_0)}$, which we must now distinguish from the normal rising hotspot area A_{hs} . We found this “initial” hotspot area using $r_{hs(t_0)} = 0.02$ kpc. We chose this value as it gave the best results when we compared the statistics of 6 MMK simulation runs done using $r_{hs(t_0)} = 0.01 - 0.06$ kpc, computed at intervals of 0.01 kpc. So in the MMK model t_0 is

$$t_0 = \left[\frac{3c_1^{2-\beta} c A_{hs(t_0)}}{(\Gamma_x + 1) (5 - \beta)^2} \right]^{1/a} \left(\frac{\rho_0 a_0^\beta}{Q_0} \right)^{3/(4+\beta)}, \quad (3)$$

with $A_{hs(t_0)} = \pi r_{hs(t_0)}^2 = \pi (0.02 \text{ kpc})^2$, ρ_0 is the central density of the ambient gas, a_0 is its scale length, β is its radial density index, Q_0 is the jet power, Γ_x is the adiabatic index of the external environment, a is $(4 + \beta) / (5 - \beta)$, and c_1 is a model dependent (but weakly varying) constant (see BW for details). The MMK model otherwise follows the prescription of the original MK model as described in §3.4 of BW.

Kaiser (2000, K2000) proposed a modification to the KDA (Kaiser, Dennett-Thorpe, & Alexander 1997) model, which essentially follows the formulation in KDA but which has the following differences. The Kaiser & Alexander (1997) and the KDA model considered a cylindrical geometry for the cocoon, where the hotspot pressure p_h drives the source expansion along the jet axis and the expansion perpendicular to the axis is governed by the cocoon pressure p_c . Hence it was assumed in the KDA model that

$$\frac{p_h}{p_c} = 4R_T^2, \quad (4)$$

where R_T is the axial ratio, or the ratio of the length of the source to the full width of a lobe half way down the jet. In subsequent studies of the shocked gas flow between the bow shock and the cocoon, Kaiser & Alexander (1999) empirically fitted (p_h/p_c) as functions of β and R_T . Such investigations appeared to show that the ratio in Eq. (4) was an overestimate. To correct this problem K2000 claimed that a better empirical formula was given by

$$\frac{p_h}{p_c} = (2.14 - 0.52\beta) R_T^{2.04 - 0.25\beta}. \quad (5)$$

The source birth function over redshift,

$$\rho(z) \propto \exp \left[-\frac{1}{2} \left(\frac{z - z_0}{\sigma_z} \right)^2 \right], \quad (6)$$

is the common gaussian functional form of all the Radio Luminosity Functions (RLFs) we considered. A peak redshift of $z_0 = 2.2$, and a standard deviation of $\sigma_z = 0.6$, following Willott et al. (2001), was adopted in the model simulations we performed in BW and in most of this paper. To explore the effect of different assumed redshift distributions we also considered extensively the RLF given by Grimes, Rawlings, & Willott (2004), which has $z_0 = 1.684$ and $\sigma_z = 0.447$, using the two-population generalised luminosity function from Table 5 of Grimes et al. (2004).

3. Model Results

3.1. $[P-D]$ Tracks

The power (P) vs. linear-size (D), or, $[P-D]$ tracks of the MBRW, MMK, and K2000 models, as well as those of the original BRW, MK, and KDA models are shown in Fig. 2. The modified models follow the same general trends as do the original models described in §5.1 of BW. The tracks are generated using the modified models (described in §2) with the default values of parameters for dynamical and power evolution from each of the original models (given in Table 1 of BW). Each source was evolved at frequency $\nu = 151$ MHz. For this figure the total linear sizes were converted to the projected sizes assuming an average viewing angle to the line of sight of 39.5° (following KDA).

The rates of steepening of the tracks are significantly different in the three new models. The MBRW track is less steep than the original BRW track. Among the three original models, KDA, BRW and MK, BRW gave the worst fit to the data, when compared with respect to K-S statistical tests (BW). If the reason for this can be identified with the fact that BRW gave the steepest $[P-D]$ tracks (Fig. 1 of BW), then this “shallowing” of the tracks in the MBRW model would imply that the K-S statistical fits to the data should be better for the MBRW model (which is indeed true). The MMK track is slightly steeper than the original MK track, implying less of a difference between their fits to the data. The K2000 track is much flatter than the corresponding typical tracks of any other model.

The “youth–redshift degeneracy” (e.g., Blundell & Rawlings 1999) is clear in these $[P-D]$ tracks. A high-power, high-redshift, source shows a faster fall off in its specific 151 MHz luminosity with time, and can even fall below the limiting flux of a radio survey at a younger age, as compared to a lower-power source at a lower z .

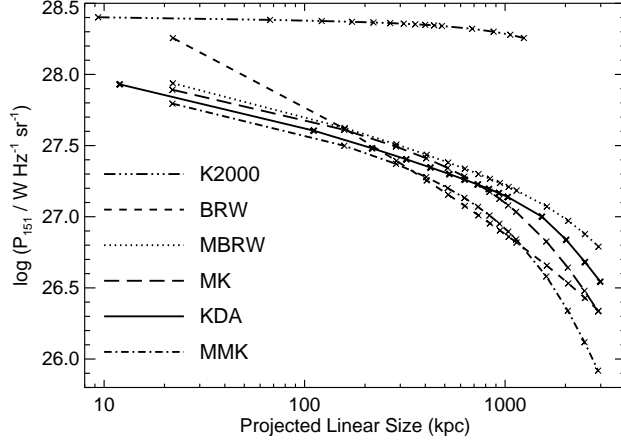


Fig. 2.— $[P-D]$ tracks of a fiducial source having jet power, $Q_0 = 1.3 \times 10^{39}$ Watts, and at redshift, $z = 0.5$. The curves of different linestyles correspond to the tracks predicted by different models as labeled. The crosses on each track denote source lifetimes of 1, 10, 20, 30, ..., 90, 100, 150, 200, 250, 300 Myr.

3.2. Preliminary Statistics: 1-D K-S Tests

We used 1-dimensional Kolmogorov-Smirnov (1-D K-S) statistics as a first quantitative test. Each of the distributions of key characteristics $[P, D, z, \alpha]$ of the radio sources detected in the simulated surveys were compared to those of the sources in the real radio surveys 3C, 6C, and 7C. The K-S probabilities, \mathcal{P} , that the two data sets being compared are drawn from the same distribution function, were taken to be figures of merit of each simulation. To quantify the overall success of a model, we added the K-S probability statistic for comparisons of P, D, z, α (i.e., $\mathcal{P}(P) + \mathcal{P}(D) + \mathcal{P}(z) + \mathcal{P}(\alpha)$) for the three surveys, weighting the statistic of a survey by the square-root of the number of simulated sources detected in that survey, and denote this overall figure of merit as $\mathcal{P}_{[P,D,z,\alpha]}$. The second figure of merit we employ, denoted $\mathcal{P}_{[P,2D,z,\alpha]}$, adds the K-S statistic probabilities for P and z to twice those for D , i.e. $\mathcal{P}(P) + 2\mathcal{P}(D) + \mathcal{P}(z) + \mathcal{P}(\alpha)$ using the same weighting method. More details can be found in §5.2.1 of BW. For each model some parameters were chosen as “better” (in providing 1-D K-S fits to the data); for these, further simulations and additional statistical tests (§3.3 and 3.4) were done.

The procedures followed in doing the simulations and in presenting the results are briefly discussed below; for complete details see §5 of BW. Table 1 gives our results for the MBRW model; Table 2 gives those for the MMK model, and Table 3 those for the K2000 model. The tables follow the same format and pattern as the corresponding tables 3, 4 and 5 of BW

for the original models, and should be compared to them. All the statistical test (K-S and correlations) results for the modified models include a 1 kpc cutoff of source size, i.e., the statistics are calculated by excluding sources with linear size, $D < 1$ kpc (see §5.2.3 of BW).

An initial ensemble, generated using the default parameters from BRW for the RG population generation, was evolved according to each of the modified models (MBRW, MMK and K2000). The sources in the simulated surveys (produced according to the prescription of §4.3 of BW) were compared to the data samples of the 3C, 6C and 7C catalogs. We examined the 1-D K-S test statistics of the first entry (the very first 3 rows) of Tables 1, 2 and 3 (modified model results) and compared those to the first entries of Tables 4, 5 and 3 of BW, respectively (original model results). From this single comparison we find that the MBRW model is significantly better (the combined 1-D K-S probabilities are $\sim 10 - 20$ times higher, which is $\sim 4\sigma$ better) than the original BRW model, while the default MMK model is only slightly better than the original MK model. The K2000 model produces much worse K-S fits than did the original KDA model, and for the reasons discussed in §4 we did not explore the K2000 variation any further.

In search of further improvements of the combined 1-D K-S statistics, we varied the beam power distribution function of the sources generated in the initial population by checking steeper exponents, x , in the power-law of the initial jet power distribution, where, $p(Q_0) \propto Q_0^{-x}$ between Q_{min} and Q_{max} . For the MBRW model the overall statistics improved the most for $x = 3.0$, while for the MMK model $x = 2.6$ gave better fits. These values of x were then used for the later simulations.

The initial population generated with $x = 3$ (but otherwise using the BRW prescription), was evolved according to the MBRW power evolution model. The corresponding 1-D K-S statistics are given in the third entry in Table 1, and show the improved fit (compared to the first entry of that table). To search for possible further improvements we varied the other parameters prescribing the power evolution in the models. Simulated surveys were constructed using the parameter listing given in Table 1 (each variation done one at a time) of the MBRW power evolution model. The total 1-D K-S statistics, $\mathcal{P}_{[P,D,z,\alpha]}$ and $\mathcal{P}_{[P,2D,z,\alpha]}$, as seen from Table 1, are comparable to or better than the original BRW model results (Table 4 of BW).

In order to find the best-fit maximum RG age, we performed simulation runs using initial populations with $x = 3$ (for MBRW), and $x = 2.6$ (for MMK), and then varied T_{Max} . The T_{Max} that gave the highest mean values of the combined statistics ($\mathcal{P}_{[P,D,z,\alpha]}$ and $\mathcal{P}_{[P,2D,z,\alpha]}$) was chosen as the best maximum age at the considered x . In the MBRW model the highest mean statistics were seen at $T_{Max} = 300$ Myr. The MMK model performed its best at $T_{Max} = 150$ Myr. Hence we used initial populations with the above “optimal” x and

T_{Max} pairs for each model in subsequent runs. The 1-D K-S results of a subset of the first set of runs employing these “optimal” initial populations and ages but varying some of the power evolution model parameters to alternate values are in Tables 1 and 2 for the MBRW and MMK models, respectively.

Upon examining these preliminary results, only those cases that gave any improvement in statistics over the default case or were essentially as good as the default were considered further. For these parameter sets three more runs (making a total of four) were done using the same large population but with different pseudo-random seeds, yielding different ensembles of simulated samples. Then the means and standard deviations of the relevant 1-D K-S statistics were found. Some “2-change” cases, i.e., models where two “superior” parameter variations (those giving high 1-D K-S probabilities) were simultaneously employed also were explored. As seen from the tables showing the individual 1-D K-S statistic probabilities (Tables 1 and 2), often several of the 12 K-S probabilities for some cases give acceptable fits, and a few would give very good fits, but it is difficult to find a single model where all are good fits. In other words, the modified models also do not give good *simultaneous* fits to the $[P, D, z, \alpha]$ data from all three of the radio surveys considered (3C, 6C and 7C).

The 1-D K-S statistical test results for the simulation runs of different models using the Grimes et al. (2004) RLF are given in Table 4.

3.3. 2-D K-S Tests

We performed additional statistical analyses on the modified models, so as to make more robust comparisons both between them and with the original models. This was done in a fashion similar to that of §5.3 of BW for the original BRW, KDA and MK models. For each modified model the 1-D K-S best-fit parameter variation cases, i.e., those which gave the highest combined probability $\mathcal{P}_{[P, D, z, \alpha]}$, according to the results from the previous sub-section were selected.

The 2-D K-S test results for both the default versions of the modified models and the parameter sets (denoted as “varied”) giving the highest total 1-D K-S probability for each model, are given in Table 5. The results are listed in a similar way as are the 1-D K-S statistics in previous tables, and are discussed below (§4.1).

3.4. Correlation Coefficients

Spearman partial rank correlation coefficients were calculated for those cases for which the 2-D K-S tests were done. We combined the $[P, D, z, \alpha]$ data from the 3 surveys: 3C, 6C and 7C III, for the actual observations and for the model simulations, and computed correlations between them (see §5.3.2 of BW for the limitation to 7C III). This was mainly done in order to subdue the tight $[P-z]$ correlation present in a single flux-limited complete survey, and to thereby discover any correlations which exist between the other source characteristics.

Table 6 gives the four-variable Spearman partial rank correlation coefficients ($r_{PD,z\alpha}$, $r_{Pz,D\alpha}$, etc.) which were computed on the combined data and on the simulated results from the modified models. We also examined the corresponding 2-variable and 3-variable correlations. Probably the most important result is that the 2-variable correlation, r_{PD} , is always negative; however, when the 4-variable correlation between P and D is found, (i.e., with the effects of z and α removed), a small positive correlation is seen between P and D (i.e., $r_{PD,z\alpha} > 0$). These are the same as trends seen in the $[P-D]$ correlations for the original models.

4. Discussion of Simulation Results

The K2000 model produces very flat $[P-D]$ tracks (Fig. 1) and the 1-D K-S statistical results obtained in the multi-dimensional Monte Carlo simulations (Table 3), are all very poor compared to any of the other models studied here or in BW. So we conclude that the K2000 model cannot well reproduce the trends of observed properties in the low frequency radio surveys. The reason for such poor behavior of this model appears to be that the K2000 model was designed specifically to describe the environments and ages of three local, and rather atypical, FR II sources. As this model is biased toward describing special environments, the parameters used in K2000 cannot really be applied globally and hence it is not surprising that this model cannot explain the cosmological evolution of RGs. Since this aspect is the crux of our investigations, we do not consider the K2000 model any further.

The primary modification made to the other models, the incorporation of a growing hotspot size, produces the following major results. The MBRW model (results in §3.2, Table 1) is a substantially better fit to the data than the original BRW model (§5.2 in BW), as the total 1-D K-S probability is better by $\sim 4\sigma$ in the default case, and by $\sim 2.5\sigma$ in the “best-fit” case, of MBRW when compared to BRW. The 1-D K-S probabilities for α are sometimes better (especially for 7C) and in a few cases (see appendix of Barai 2006) approach the value 0.01 for which a model spectral index fit is not firmly rejected. The

MMK model produced fitting statistics (§3.2, Table 2) which are better than or comparable to the original MK model fits (§5.2 in BW).

We have explored the modified models through our extensive multi-dimensional Monte Carlo simulation procedures and parameter variations in the modified models. But similarly to what we found for the original models in §5 of BW, we found that no modified model gives acceptable fits to *all* the source characteristics, $[P, D, z, \alpha]$, for *all* the three surveys 3C, 6C and 7C, simultaneously.

Steepening the power law index for the initial beam power distribution (Eq. 2 of BW) to $x = 3$ (from $x = 2.6$ used by BRW) while using the default maximum age $T_{Max} = 500$ Myr, improved the 1-D K-S statistics for the MBRW model, as can be seen from Table 1. However, in the MMK model $x = 2.6$ gave better results, as compared to $x = 3$ (Table 2). This is the only model we examined which gave better 1-D K-S fits with the beam power distribution index set to $x = 2.6$. Simulations done by co-varying T_{Max} and x gave better fits at a maximum age of 300 Myr (MBRW) and 150 Myr (MMK), when combined with the above “optimal” values of x . These “best-fit” values of x and T_{Max} for the modified models (except x for MMK) are comparable to those found earlier for the original models (§6 of BW).

4.1. Comparing Models with Additional Statistical Tests

Examining the 2-D K-S test results given in Table 5 we can say that the $[P-z]$, $[P-D]$ and $[z-D]$ planes can be reasonably fitted by the “varied” cases of the modified models. Six of these 9 planes not involving α (those three slices for each of the 3C, 6C and 7C comparisons) had 2-D probabilities > 0.1 for the MMK “varied” model; this is true for 4 \mathcal{P} ’s in the MBRW cases. All of the 2-D \mathcal{P} ’s of the “varied” MMK model are higher than those of the default MMK. When compared to the corresponding default versions, improvements are seen for 8 of 9 of the 2-D \mathcal{P} ’s not involving α in the “varied” MBRW model. These 2-D results provide support for the superiority of the “varied” models (selected from 1-D K-S tests) in fitting the data.

Comparing the “varied” cases of the two modified models themselves in the 9 planes not involving α , we see that 6 of the 2-D \mathcal{P} ’s for the MMK model are higher than those of MBRW. Nonetheless, the α -related 2-D K-S probabilities are ≤ 0.008 for every modified model. So, similarly to the original models, the modified models cannot fit any plane involving α . From the 2-D K-S probabilities we conclude that the MMK model is better (having the highest number of 2-D \mathcal{P} ’s close to 1) in fitting the observational data than is the MBRW model.

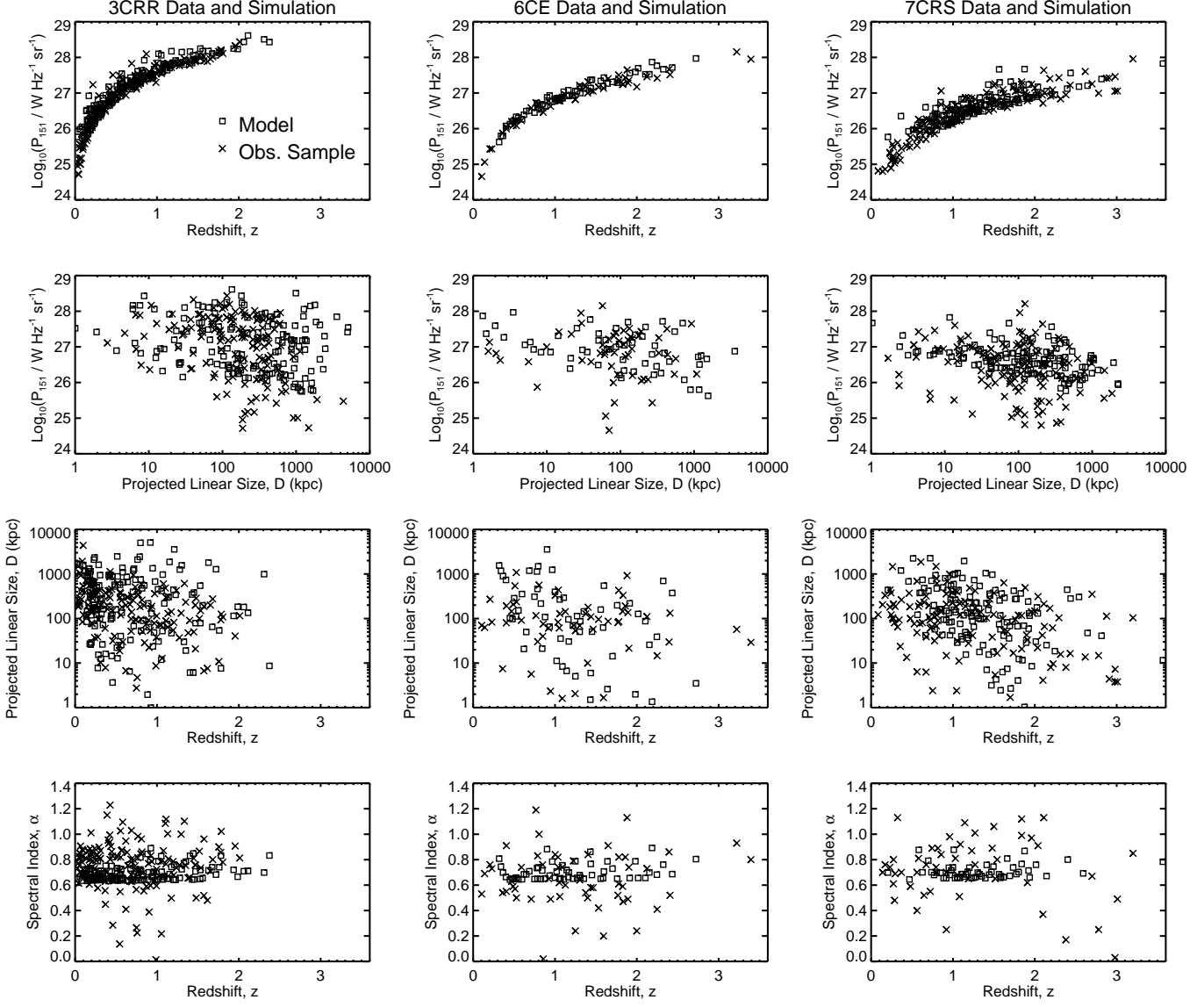


Fig. 3.— The 3CRR, 6CE and 7CRS survey data, overplotted with the $[P-D-z-\alpha]$ planes for the 3C, 6C and 7C simulations of a good fit of the MBRW model. The initial ensemble (of size 4963343) is generated using $x = 3.0$, $T_{Max} = 300$ Myr; the power evolution is with the parameter variation of $t_{bf} = 100$ yr, with the rest being their default values as in the MBRW model (§2). The 1-D K-S statistics for this case are in Table 1 (last but 6th entry).

From the Spearman partial rank correlation analyses on the combined data of the 3 surveys (Table 6) we conclude that many matches to the data correlations are acceptable for the MBRW model, but they are less good for the MMK model. It is interesting to note

that the parameter variation cases which were the best fits (i.e., gave the highest combined probability, $\mathcal{P}_{[P,D,z,\alpha]}$) from the 1-D K-S results, or the “varied” cases in Tables 5 and 6, are not necessarily the best fits according to the correlation analyses. For the MBRW and MMK models the default and the “varied” cases perform comparably, as 3 correlations are better in the default, and the remaining 3 are better in the “varied”, models.

Considering the signs of the four-variable coefficients of the combined surveys, the MMK model predicts a $[P-\alpha]$ anti-correlation, a $[D-z]$ correlation; its “varied” case also produces a $[P-z]$ anti-correlation. All these are trends opposite to those seen in the survey data and to the other models, except that the MBRW model also predicts a $[P-\alpha]$ anti-correlation. Both the MMK models are the only ones which produce the correct signs of the $[D-\alpha]$ and $[z-\alpha]$ correlations of the combined survey data (the $[D-\alpha]$ correlation is also exhibited weakly by the MBRW default case). However, this advantage is not meaningful as the MMK model gives very poor fits to the actual α -distributions.

According to the correlation coefficient analyses involving the data from all the surveys (3C, 6C and 7C) the the MBRW model fits the data most closely, followed by MMK. In particular, the MBRW model provides the best fit to the key 4-variable correlation, $r_{PD,z\alpha}$. This indicates that in the BRW model a growing hotspot is able to reproduce the $P-D$ evolution (seen in 3C, 6C and 7C survey data) better than assuming a constant hotspot size (the original BRW model). Similar trends emerged when we examined the 3-variable correlation coefficients.

4.2. $[P-D-z-\alpha]$ Planes

We plotted planes through the $[P-D-z-\alpha]$ volume for the simulated surveys using the modified models, and compared them with the overall trends in the $[P-D-z-\alpha]$ slices of the observational data. The actual 3C, 6C and 7C data are plotted as crosses and the simulated data (3C, 6C and 7C virtual surveys) for the “best-fit” or “varied” parameter set for the MBRW model (those which give the highest total 1-D K-S probability) are overplotted as squares in Fig. 3. The Monte Carlo results for the “best-fit” parameter set for the MBRW model are shown in Fig. 4. The main features of the $[P-D-z-\alpha]$ planes of the modified models are analogous to those of the original models in §6 of BW, so we discuss them only briefly, placing stress on any new features.

In the $[P-z]$ plane, all of our simulated surveys of all the modified models miss many of the low- P sources seen in the data. Too few low- z /low- P sources are produced in all the simulated 7C surveys. There is underproduction of very high- z sources ($z > 2$) in the 7C

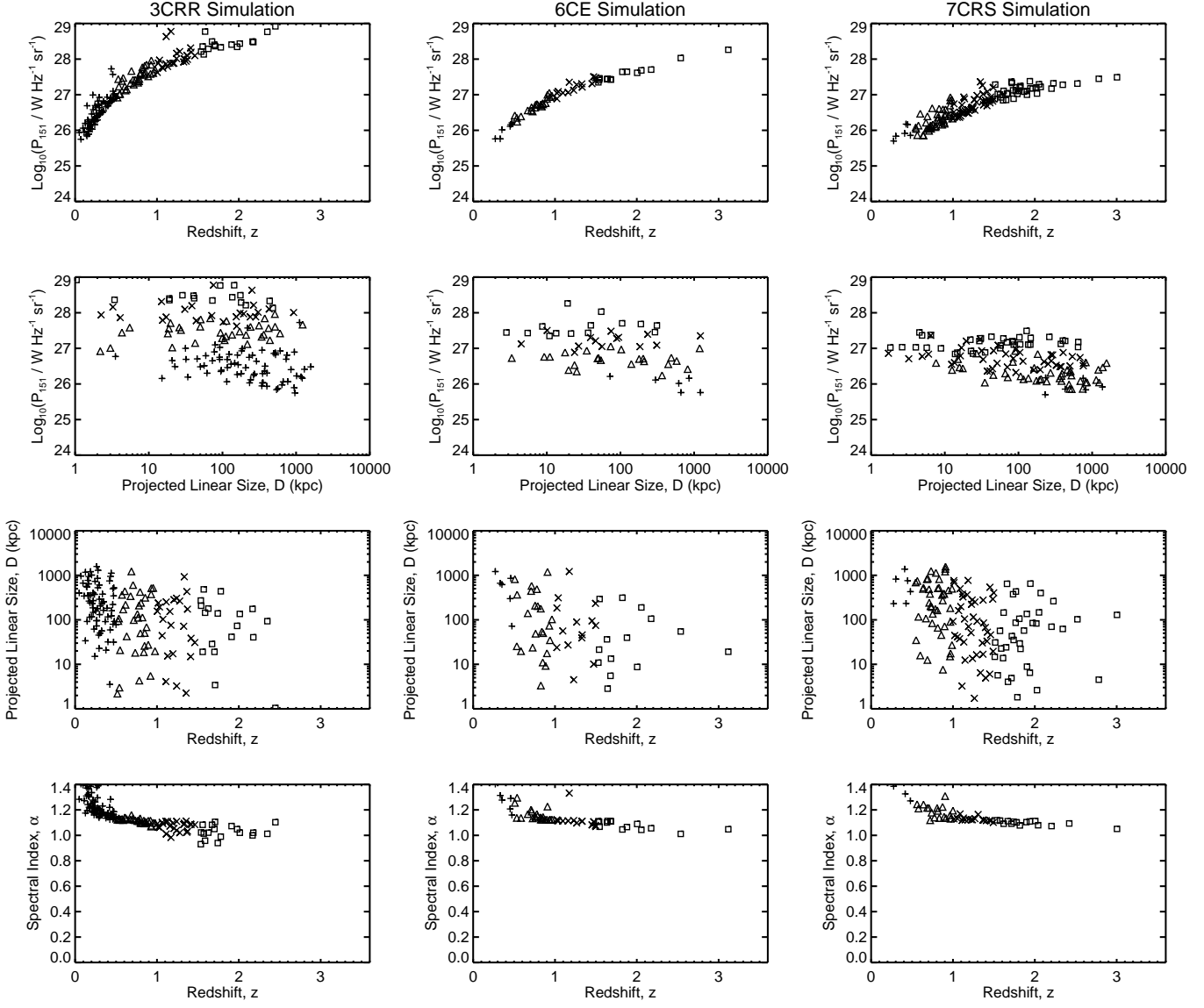


Fig. 4.— The $[P-D-z-\alpha]$ planes for the 3C, 6C and 7C simulations of a good fit of the MMK model. The initial ensemble (of size 3888492) is generated using $x = 2.6$, $T_{Max} = 150$ Myr; the power evolution is with parameter variation $\beta = 1.6$, the rest of the parameters having their default values of the MMK model (§2)). The symbols classify the sources into redshift bins as follows; *Plus*: $0 \leq z < 0.5$, *Triangle*: $0.5 \leq z < 1.0$, *Cross*: $1.0 \leq z < 1.5$, *Square*: $1.5 \leq z$. The 1-D K-S statistics for this case are in Table 2 (9th entry).

simulations and a similar, but less pronounced, trend is also present for 6C.

From the trends in the $[P-D]$ plane, the MBRW model overproduces large powerful

sources in 3C, and underproduces the large weaker sources. The 6C and 7C [P – D] planes of all the modified models show a closer match to the data, but the actual data is more scattered than the simulations. Given that any additional physics not included in the models would tend to broaden this distribution, this result is expected.

There is P – D anti-correlation in the MMK model in all of the 3C, 6C and 7C simulations. Such P – D evolution is also seen in the MBRW model where it is more pronounced in the 6C and 7C simulations. An important improvement in the MBRW model is that the strong P – D anti-correlation apparent in even the “best-fit” BRW model is diluted when modified to incorporate a growing hotspot.

In the [D – z] plane, the MBRW model still overproduces the larger 3C sources. The MMK model’s “best-fit” case [D – z] planes seem to be a good fit to the data (especially the 3C [D – z]), with about the right amount of D – z anti-correlation. The MBRW model produces a weaker D – z anti-correlation than does the data in 3C, but one stronger than in the data in 6C and 7C. An explanation of the D – z evolution as an effect of the “youth-redshift degeneracy” was given while discussing the original model planes in §6 of BW. From these trends we conclude that the MMK model is the best fit (by eye) to the [D – z] planes of the 3C, 6C and 7C data.

All the other characteristics examined in the simulations show tight correlations with the spectral index. The data shows much greater scatter in α than is seen in any of the models. The spectral index distributions of all the model simulations are similar to those in BW. Since the α statistical fits are very poor, we do not discuss them any further.

4.3. Alternative RLF

The Grimes et al. (2004) RLF is tested using different values of x and T_{Max} , but with the default values of radio lobe power evolution model parameters of the different models. When comparing the simulations using Grimes et al. (2004) RLF with respect to those with Willott et al. (2001)’s (with the same model parameters otherwise), most of the models give better 1-D K-S statistics using Willott et al. (2001)’s RLF. The KDA and MK models are better for 5 out of 6 comparisons, the MBRW model is better for 4 out of 6 total. The MMK model performs equally using both RLFs. The BRW is the only model which give better results using Grimes et al. (2004) RLF for all 5 comparisons we made.

So we conclude that the KDA, MK and MBRW models give better fit to the data using Willott et al. (2001)’s RLF. From the runs we performed the MMK model produces comparable results with both the RLFs. The BRW model is better fit with the Grimes et al.

(2004) RLF, but in an absolute comparison with the other models (KDA, MK and MBRW), the fits are still poor.

All the spectral index fits are still very poor using the alternative RLF. So we can say that altering the redshift birth function has little effect on the major drawback of these models: the mismatch of the spectral index behavior between data and simulations.

5. Relevant Volume Filling Fraction

The volume of our “Relevant Universe” is taken to be the volume of the cosmic baryons which exist as the WHIM and have temperatures $10^5 < T < 10^7$ K (e.g., Cen & Ostriker 1999, 2006; Davé et al. 2001). This warm/hot intergalactic gas appears to contain a very large fraction of the baryons ($\sim 40 - 50\%$ by mass) in the universe at the present epoch. The WHIM permeates the universe as extended large-scale filamentary structures, the junctions of which are the sites of galaxy and cluster formation.

To calculate the volume fraction of the relevant universe filled by RGs we first consider that the initial ensemble of sources generated to yield the simulated surveys provides a good estimate of the actual population of RGs at different redshifts since, as discussed above, those Monte Carlo simulations do produce decent fits to the P – D – z distributions. Among the millions of RGs generated in such an ensemble, only a few tens to hundreds are detected in the simulated surveys. The key point is that this is also what happens in reality: among the millions of RGs born through the quasar era, we can now detect only a few in our flux-limited and redshift-complete radio surveys. Severe energy losses (adiabatic, synchrotron and IC losses) conspire to force the vast majority of all RGs to fall below our observational flux limits, as discussed in detail in earlier work (Gopal-Krishna, Wiita, & Saripalli 1989; Blundell & Rawlings 1999; BRW; GKW01; GKW03a,b; GKWO; GKWB04). Such power losses are evident in the simulations from the steeply falling [P – D] tracks of §3.1.

Next, the universe is divided into redshift bins (shells), and the relevant volume fraction is calculated in each z -bin. Let the minimum and maximum redshifts of a shell be z_{min} and z_{max} . The bin-width is taken as $\Delta z = 0.02 = (z_{max} - z_{min})$. The mid-redshift of a bin, $z_{mid} = (z_{min} + z_{max})/2$, is considered as the epoch of that bin. Then, the distribution of the volume fraction is estimated as a function of redshift, which is then integrated over the entire quasar era epoch to get the total volume contribution of several generations of RGs in the universe.

5.1. Volume of WHIM in the Universe

We use a consensus flat, dark-energy dominated universe (Spergel et al. 2003, 2006), with Hubble constant $H_0 = 71 \text{ km s}^{-1} \text{ Mpc}^{-1}$, matter density parameter $\Omega_M = 0.3$, and vacuum energy density parameter $\Omega_\Lambda = 0.7$. The comoving volume over all-sky ($4\pi \text{ sr}$) in a redshift shell of the universe between z_{min} and z_{max} is (Hogg 1999),

$$\Delta V_{co} = \frac{4\pi}{3} \left(\frac{c}{H_0} \right)^3 (\chi_2^3 - \chi_1^3), \quad (7)$$

where,

$$\chi_{2,1} = \int_0^{z_{max}, z_{min}} [\Omega_M (1+z)^3 + \Omega_\Lambda]^{-1/2} dz. \quad (8)$$

Our big ensemble (initial population) explicitly detects sources over the 3CRR sky survey area, $\text{Area}_{3C} = 4.23 \text{ sr}$. So the RG population from which these sources are detected lies within a smaller comoving volume extending over only the 3CRR sky area, since in these simulations the number of sources can be taken as proportional to the sky area over which they are surveyed. If a simulation detects $N_{\text{sim}(3C)}$ sources, where there are $N_{\text{samp}(3C)} = 145$ sources in the real 3CRR survey, then the 3C detection ratio is written as, $\text{Ratio}_{3C} = N_{\text{sim}(3C)}/N_{\text{samp}(3C)}$. Hence the comoving volume over the effective 3C survey area is,

$$\Delta V_{co,3C(\text{eff})} = \Delta V_{co} \frac{\text{Area}_{3C} \times \text{Ratio}_{3C}}{4\pi}. \quad (9)$$

The effective comoving volume of the z -shell is then converted to the proper volume it had at that epoch, as $\Delta V_{prop} = \Delta V_{co,3C(\text{eff})} / (1+z_{mid})^3$. The effective relevant volume of the z -shell is then the fraction of the proper cosmological volume of the shell occupied by WHIM.

The WHIM volume fraction, ξ , is adopted from the large-scale cosmological simulations of Cen & Ostriker (1999). Cen & Ostriker (2006) give an improved WHIM fraction calculation by explicitly including galactic superwind feedback processes, but for our purposes there is no significant difference from their previous results. Hence we obtain the final “relevant volume of the universe” inside a z -shell, $\Delta V_{WHIM} = \xi \Delta V_{prop}$.

5.2. Radio Galaxy Volumes and Relevant Fraction

We calculate RG volumes by assuming that the RGs are cylindrical in shape with total length $D(t)$ (Eq. 4 of BW), at an age t . The axial ratio, R_T gives the ratio of the source length and its width (or diameter). The volume occupied by a RG at an age t is,

$$V_{RG}(t) = \pi \left[\frac{D(t)}{2R_T} \right]^2 D(t) = \frac{\pi D(t)^3}{4R_T^2}. \quad (10)$$

To get a conservative estimate, in all the volume computations $R_T = 5$ is used, irrespective of the model (unless otherwise noted). This value appears to be an upper bound to the average axial ratio based on observations (GKW01 and references therein). The difference between this choice of $R_T = 5$ used to calculate the volumes, and that in the KDA model, where $R_T = 1.3$ gave the best fit to the $[P\text{--}D\text{--}z]$ planes, is noteworthy. If later work shows that $R_T < 5$ is indeed preferable, then a typical radio galaxy volume $V_{RG}(t)$ will be bigger, by up to a factor of ~ 15 , thus more strongly favoring the picture of substantial cosmological impact of RGs.

Following the conservative bent of GKW01, we only consider the contributions of the more powerful FR II RGs despite the fact that the weaker FR I RGs are much more numerous in our local universe and some of them are also seen to extend for hundreds of kpc. There are several good reasons for making this approximation, although we cannot precisely quantify its effect. First, the Willott et al. (2001) RLF indicates that the numbers of FR I and FR II sources were much more comparable during the quasar era on which we are focusing, with the lower luminosity sources hardly evolving for $z > 0.7$ while the higher luminosity sources continue to rise in density with z until $z > 2$. Second, it is very likely that the efficiency with which jet thrust is converted into radio flux in FR I's is substantially higher than in FR II's (e.g., Gopal-Krishna & Wiita 1991; Baum, Zirbel, & O'Dea 1995), so that a jet of equal power would make a brighter FR I source, thereby skewing the RLF of FR I's upward. But since the typical FR I has much lower radio flux it is being energized by very much weaker jets than those powering a typical FR II. Hence, on average, the volumes enclosed by individual FR I's will be substantially lower than those of the FR II RGs considered here. In addition, since the expansion of FR I's is less rapid they produce weaker (if any) shocks for shorter times and will have less ability to trigger star formation.

Let the cosmic times of the boundaries of the z -shell be denoted as t_{in} and t_{out} (corresponding, respectively, to z_{min} , z_{max}). We assume that all the RGs in an ensemble live out to their full lifetime, T_{Max} . So, while the vast majority of FR II radio sources ever born are too faint to be detected now, they do expand as long as the AGN is feeding the jets and lobes and hence contribute to filling part of the universe. We count all the RGs in the simulation initial ensemble which have any portion of their lives falling in the time range of that z -bin. The volume contribution of all the RGs which are intercepted by a z -shell are then added to get the total RG volume, ΔV_{RG} . The relevant volume fraction in a z -shell is $\Delta\iota(z) = \Delta V_{RG}/\Delta V_{\text{WHIM}}$. Integrating $\Delta\iota(z)$ over z gives this volume fraction as,

$$\iota = \int_0^{z_{early}} \Delta\iota(z) dz, \quad (11)$$

where z_{early} is the earliest redshift of a source in the initial ensemble.

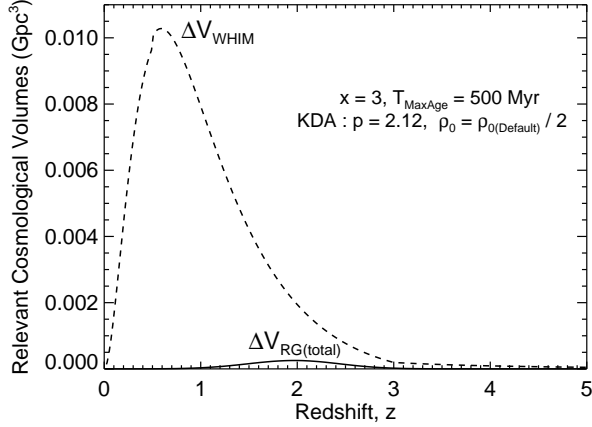


Fig. 5.— Relevant volumes in the Universe: WHIM volume over the effective 3CRR sky area, and total RG volume, for the model with parameters noted as a function of redshift.

There is another significant factor which must be taken into account to estimate the total fraction correctly; this arises from the contributions of the several generations of RGs during the quasar era (QE). The total volume filled by the multiple generations of RGs in the universe over the whole QE was roughly taken into account in GKW01. They considered the length of the QE as $t_{QE} \sim 2$ Gyr, and the maximum age of radio sources $T_{Max} = 500$ Myr. We also adopt this rather large maximum length of AGN activity in some of our simulations, as it was suggested by BRW. Ages of that order are supported by a variety of recent observational studies mentioned in §2 of BW; the most recent modeling of RG ages by Machalski et al. (2006) also implies high values for T_{Max} . GKW01 argued that every place in the universe could have been potentially affected by $t_{QE}/T_{Max} = 4$ generations of RGs during the entire QE. So they multiplied the mean of the corrected RLF by (t_{QE}/T_{Max}) to get the total proper density of intrinsically powerful radio sources in the universe.

In our simulations we obtain the total fraction by adding the values of $\Delta\iota(z)$ several times in intervals of T_{Max} over the entire QE. The length of the QE is obtained from the temporal length of the epoch for which $\Delta\iota(z) \geq 5\%$ of its peak value. Starting from the high- z end-point of the QE, values of $\Delta\iota(z)$ are computed at intervals of T_{Max} and summed, until the low- z end-point of the QE is reached or exceeded. This addition is done several times; each time the starting point is chosen differently by going back or forward from the original starting point by integral multiples of 50 Myr. The summed $\Delta\iota(z)$ obtained from these several additions (each starting from a different cosmic time), are then averaged to get the mean total “relevant volume fraction”, ζ , of the universe filled by generations of radio galaxies during the quasar era.

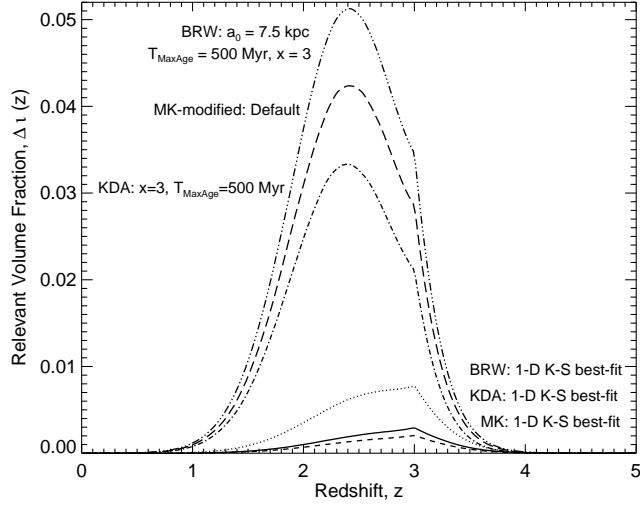


Fig. 6.— Relevant volume fractions of the universe filled by radio galaxies from several model simulations. The vertical alignment of the labels correspond to those of the model plots.

5.3. Results and Discussion

The relevant volume fraction, ζ , was computed for a subset of the model simulations done with the 3 main models, KDA, BRW and MK, as well as for the modifications we have considered in the present work.

We now consider the model parameters which determine the relevant volume fraction. The distribution functions of RG z (Eq. 6: z_0, σ_z), and of jet power (Eq. 2 of BW: x, Q_{min}, Q_{max}), according to which an initial ensemble of sources are generated following the prescription from BRW, along with the maximum age, T_{Max} , are the parameters which are model-independent in the sense that they do not depend on the RG lobe power evolution models. The RG volume, $V_{RG}(t)$ (Eq. 10) depends on the models through the linear size, $D(t)$ (Eq. 4 of BW), which explicitly involves the ambient density parameters (Eq. 3 of BW: ρ_0, a_0, β). The other model-dependent factor is the detection ratio (§5.1) which is obtained from the number of sources in the simulated surveys.

5.3.1. Cosmological Volumes vs. Redshift

In Fig. 5, the *dashed* curve is the final relevant WHIM volume ΔV_{WHIM} (§5.1), and the *solid* curve is the total RG volume (ΔV_{RG} , §5.2), for a case of the KDA model. The

RLF or redshift distribution from which the sources in the initial ensemble are drawn is a gaussian, so the maximum number of sources in the initial ensemble are born near the peak at $z_0 = 2.2$. From Fig. 5 we can see that the total RG volume, ΔV_{RG} , peaks at $z \sim 2 < z_0$. This is because the majority of sources born at z_0 remain active for $T_{Max} = 500$ Myr, and are thus counted in several later z -bins. They contribute to the RG volume in increasing amounts as they grow in age, until the maximum age, T_{Max} , after which they are assumed to no longer do so. Their combined increasing contributions at later times make ΔV_{RG} peak at a $z < z_0$. This peak redshift of ΔV_{RG} should be around the cosmic epoch corresponding to $t(z_0) + T_{Max}$, as that is when the largest number of sources in the population reach their maximum volumes.

On the other hand, Fig. 6 shows that the relevant volume fraction, $\Delta\iota(z)$, peaks at $z > z_0$. The distribution of WHIM volume, ΔV_{WHIM} (Fig. 5), can be invoked to explain this result. We see that ΔV_{WHIM} rises sharply from $z \sim 3$, until it reaches a peak at $z \sim 0.7$, because of the trends of proper volume of z -shells in the consensus cosmology. When the ratio of ΔV_{RG} to ΔV_{WHIM} is taken to get $\Delta\iota(z)$ at $z \sim z_0$, ΔV_{RG} is divided by a volume ΔV_{WHIM} which decreases with increasing redshift.

A representation of how the volume contribution of multiple RG generations are added to get the total cumulative fraction over the entire QE is given in Fig. 7. The solid black curve in the figure is the volume fraction $\Delta\iota(z)$ as a function of redshift. The symbols (of a single type) plotted on it are the values of $\Delta\iota(z)$ which are picked at intervals of $T_{Max} = 500$ Myr over the QE, and added. The different plotting symbols denote the different starting points for the added fractions, which were finally averaged to get the cumulative fraction, ζ . For this model of Fig. 7 (BRW default using initial ensemble with $x = 2.6$, $T_{Max} = 500$ Myr), the quasar era spans the redshift range $z_{QE} = 3.52 - 1.16$, or the cosmic time range $1.74 - 5.10$ Gyr, corresponding to a quasar era of duration $t_{QE} = 3.36$ Gyr. Hence there are contributions from ~ 7 generations of RGs in the case where $T_{Max} = 500$ Myr. The final relevant fraction results for this model are:

$$\iota = 0.0123, \quad \zeta = 0.0301. \quad (12)$$

5.3.2. Comparison Between Models

Fig. 6 shows plots of the relevant volume fraction, $\Delta\iota(z)$, as a function of redshift, for some of the model simulations. Table 7 gives the relevant volume fraction results for the models. The results for a particular parameter variation of a model are given in each row. Most of the column headings were defined earlier. Column 6 gives A_z , the normalizing factor

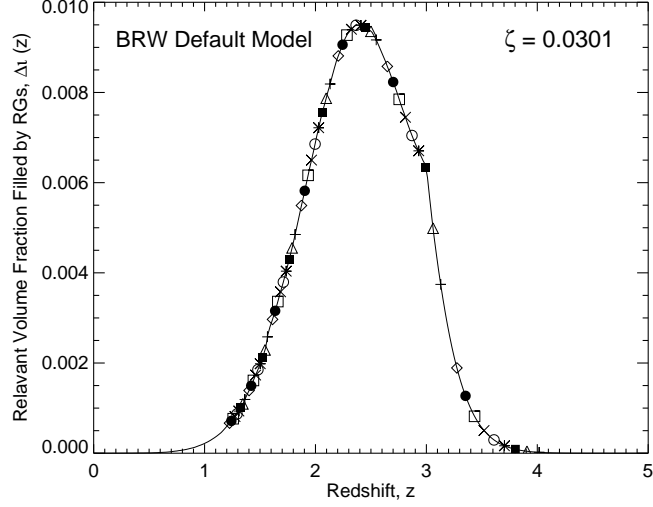


Fig. 7.— Total relevant volume fraction of the universe filled by RGs by adding the volume contributions of multiple generations of RGs over the quasar era. This is for the BRW simulation with default model parameters, for the initial ensemble of size 1561417 generated using $x = 2.6$, $T_{Max} = 500$ Myr.

in the redshift distribution (Eq. 6) which was used to generate the initial population; A_z is the factor by which $[V_C(z = 0) \times \rho(z_{birth})]$ (paragraph 5, §2 of BW) is multiplied to get the number, N_{born} , of radio sources born within the relevant comoving volume, V_C . From Table 7 we see that the fractions ι and ζ vary significantly both between the models and for different parameter sets within the same model. Quite a wide range of relevant volume filling factors can be produced by the considered ranges in model parameters.

For the “default” case, RGs in the BRW simulations cumulatively fill $\sim 3\%$ of the relevant universe, and $\sim 3.4\%$ of the relevant volume is filled in the MBRW model. This number is $\sim 4.5\%$ for the KDA, $\sim 7\%$ for the MK and $\sim 13.5\%$ for the MMK models. At the same x and T_{Max} , and using default model parameters, the MK model gives the largest relevant fractions, followed by the KDA and finally by the BRW models. This is because a larger initial ensemble needs to be generated in the MK model to yield the same number of detected sources compared to the other models.

Still, the runs involving parameter variations corresponding to “1-D K-S best-fit”s of the BRW and KDA models give higher fractions (by $\sim 4 - 5$ times) than do the corresponding “default” models, for the *same* x and T_{Max} . This is because the BRW best-fit is with $a_0 = 7.5$ kpc $< a_0$ (Default), and KDA best-fit is with $\rho_0 = \rho_0$ (Default)/2, both of which have the effect of increasing $D(t)$ and thence the RG volumes. However, when the favored lower values of

T_{Max} are employed, the cumulatively filled fractions are $0.015 < \zeta < 0.07$. The relevant volume fractions for these most preferred (with respect to K-S statistics) parameter sets are all very low compared to the estimate in GKW01, $\zeta = 53\%$. Still, for certain less likely parameter values this fraction goes as high as 16% for BRW, 55% for KDA, and 20% for MK model.

The relevant fraction is greater for higher T_{Max} (for same x), as is evident from the expression for the RG volume, which scales as $t^{9/(5-\beta)}$. For the same T_{Max} , the fraction is higher with $x = 3.0$ than with $x = 2.6$. This might seem counter-intuitive, as with a steeper jet power distribution the sum of volumes occupied by the same number of sources should be smaller. The mean RG volume at maximum age, $\langle V(T_{Max}) \rangle$ is indeed smaller (by a factor of $1.21/1.44 = 0.84$), as discussed later (§5.4). Nonetheless, a larger volume fraction at higher x can be explained as many more sources must be generated using the steeper slope ($x = 3$) to yield numbers of sources in the simulations comparable to those in the real surveys. Explicitly, to get the same Ratio_{3C} , larger ensemble sizes (by 1.5 – 3.5 times) are required for $x = 3$ than for $x = 2.6$, and the increase in ensemble size more than offsets the smaller mean volume.

5.4. Comparison of Results with a Previous Estimate

Gopal-Krishna & Wiita (2001) performed a preliminary calculation to find the relevant volume fraction added over several generations of radio sources during the quasar era. From the results in §5.3 we see that the relevant fraction obtained in this work is considerably smaller than the fraction estimated by GKW01. For the BRW default model (simulation done with initial ensemble of size 1561417 generated using $x = 2.6$, $T_{Max} = 500$ Myr) we obtained $\zeta \approx 0.03$ (2nd entry of Table 7), whereas using published graphs in BRW for the same model GKW01 obtained $\zeta \approx 0.5$.

There are six differences between the calculations, which taken together, can account for most of the discrepancy between the two calculations.

- (1) We adopted the newer consensus cosmology (e.g, Spergel et al. 2006). GKW01 used cosmologies with $H_0 = 50$ km s $^{-1}$ Mpc $^{-1}$, and with either $\Omega_M = 0$ or 1, but with $\Omega_\Lambda = 0$.
- (2) In the model simulations performed in BW and this work, we used $Q_{min} = 5 \times 10^{37}$ W as the minimum jet power, following BRW (as described in §2 of BW). GKW01 took the effective lower limit of Q_0 as $Q_m \equiv 7.5 \times 10^{37}$ W (their §2.2), which they inferred (by observing the BRW [P–D] tracks in their Figs. 13 and 14) to be the minimum power a source must have in order to appear in the BRW data set. A higher minimum Q_0 means

that the RG jets will be, on average, more powerful, thus making the total RG-volume and the relevant fraction higher.

(3) We obtained the average radio galaxy volume at maximum age $T_{Max} = 500$ Myr to be 1.44 Mpc^3 , whereas GKW01 obtained a value of 2.1 Mpc^3 (their §2.3), using the same BRW default model parameters (except for the different Q_{min} choice). Clearly, $\langle V(T_{Max}) \rangle$ should scale as $Q_{min}^{3/(5-\beta)}$, since $Q_{max} \gg Q_{min}$. So GKW01’s $\langle V(T_{Max}) \rangle$ should be higher than ours by $(7.5/5)^{3/(5-\beta)} = 1.42$.

(4) To get the total proper density of RGs, GKW01 multiplied the peak of the corrected RLF by $(t_{QE}/T_{Max}) = 4$ generations of RGs in their §2.2. We consider the contribution from multiple generations of RGs by adding the volume fractions $\Delta\iota(z)$ in intervals of T_{Max} over the entire QE (§5.2), so we more precisely take into account the distribution of $\Delta\iota(z)$ vs. z . As can be inferred from Fig. 7, simply multiplying the peak fraction (highest $\Delta\iota(z)$ in Fig. 7) by 4, which was done in GKW01, gives an overestimate of ζ by a factor of $0.038/0.030 = 1.27$.

(5) We interpolated the fractional WHIM volume in the universe, which varies with z , from the calculations of Cen & Ostriker (1999). This WHIM volume fraction decreases with increasing redshift, starting from $\simeq 0.095$ at the present epoch, to reach $\simeq 0.01$ at $z \simeq 3$. GKW01 considered a constant WHIM volume fraction of 0.03 at all redshifts of the QE. For our computation, the higher WHIM fraction at low- z dominates over the lower WHIM fraction at high- z .

(6) In converting from comoving to proper volumes GKW01 used a value of $z = 2.5$. We integrated over each value of z and had an effective average value of $z \sim 2.2$. This value is basically the peak, z_0 , of the Gaussian redshift distribution (Eq. 6) of the radio sources. This difference causes the GKW01 result for ζ to exceed ours by another factor of $\sim (1 + 2.5)^3/(1 + 2.2)^3 = 1.31$.

6. Conclusions and Future Work

We have performed comprehensive quantitative tests of extensively explored modifications to the BRW and MK models for FR II RG evolution which allowed the sources’ hotspot sizes to grow with age. We often found adequate fits to the $[P-D-z]$ distributions for each model for each of the Cambridge catalog subsamples (3CRR, 6CE, 7CRS). But we cannot locate any parameter sets which provide good simultaneous fits to all three catalogs and to all four of these observables $[P-D-z-\alpha]$. Of particular concern are the spectral indices, where none of the models provides an adequate fit. We note that all of these models only produce a single gross spectral index and that future models must improve upon the treatment of

the physics that leads to average emissions at different frequencies.

From the power vs. linear-size tracks we see that the BRW [P – D] tracks are the steepest among all six models, while the MBRW tracks are significantly less steep. This causes the most significant change found in the model performances after modification, in that the MBRW model gives substantially better K-S statistical fits to the data than the BRW model.

All the models produced better statistical fits with the slope of the jet power distribution set to $x = 3$, except the MMK model which performed better with the default value from BRW, $x = 2.6$. Considering the active lifetime of the AGN for which the jets feed the lobes, we found that all the models gave better fits with T_{Max} between 150 – 300 Myr; the high default value of 500 Myr is disfavored.

The KDA, MK, MBRW and MMK models all perform comparably in terms of producing high values of total 1-D K-S probabilities. From the 2-D K-S test results the “varied” cases of most of the models can produce adequate fits to the [P – z], [P – D] and [z – D] planes. Sorting all the models in descending order of the number of non- α 2-D \mathcal{P} ’s greater than any other model we have: KDA, MK, MMK, MBRW, BRW. From the 4-variable Spearman partial rank correlation coefficient analyses, we find that the original KDA model can match the survey data correlations very closely (at least for P , D and z), followed by BRW and MBRW, then finally the MK and MMK models.

The existing redshift complete radio source catalogs can limit the allowed parameters for each of the models individually and can show that the K2000 model is not a good fit to the ensemble of RGs. However, they are too small to make a clear distinction among the models we have tested. A significant range of the models can provide adequate descriptions of the [P – D – z] distributions. Only by obtaining redshift-complete samples covering significantly larger portions of the sky than those studied in the 6C and 7C surveys would the data have enough power to positively discriminate among the models.

A major goal of this work has been to calculate what fraction of the “relevant universe”, or the large-scale filament-structured WHIM volume, do the FR II RGs born over the quasar era cumulatively occupy. We found that quite a wide range of relevant volume filling factors can be produced, with certain choices of parameters in our simulations producing relevant filling factors as high as $\sim 20\%$ and even $\sim 50\%$; however, none of these models provide good K-S statistical fits to the observations and hence these rather high filling factors are unlikely to be realistic. For both the default and 1-D K-S “best-fit” cases of the models using the best values of T_{Max} the cumulative volume filling fraction of several generations of RGs varied within the range $\sim 1.5 – 7\%$. These volume fractions are significantly smaller than the preliminary estimate of GKW01.

We infer that FR II RGs probably cover $\sim 5\%$ of the WHIM volume cumulatively over the quasar era. Such filling factors were produced by models providing the best statistical fits to the observations, which are quite good fits to the P – D – z distributions, so they are likely to be close to the most probable “real” fractions. Still, despite the large number of models we have examined they are not numerous enough to allow a proper error estimate on this key quantity. The fractional “internal” errors on these filling factor values, as obtained by computing results for several of the same models and same parameter values but with different initial random seeds, were in the range $0.017 < \sigma/\langle \zeta \rangle < 0.10$.

We conclude that the expanding radio galaxies born during the quasar era can play a significant, though probably not dominant, role in the cosmological history of the universe through the triggering of extensive star formation and the spreading of magnetic fields.

Recently Blundell et al. (2006) provided observational evidence for the discovery of low-energy cutoff of particle acceleration in the lobe of a giant FR II RG. They obtained a value of $\gamma_{min(hs)} \sim 10^4$ as the minimum Lorentz factor of particles in the hotspot, substantially higher than the values in the models where (1–10). Investigating models using such (tentatively) observationally supported higher $\gamma_{min(hs)}$ values will be a worthwhile venture.

In a recent study Kawakatu & Kino (2006) described the dynamical evolution of the hotspots of radio loud AGN using a model significantly different from that of KDA. Incorporating such evolving hotspots into the models of radio lobe power evolution we analysed would be an interesting modification to the models worth exploring.

A potential indicator which can provide an excellent test of whether RGs do really trigger galaxy formation, is the 3-point correlation function between radio galaxies in large scale galaxy (redshift) surveys (e.g., Borderia et al. 1991). If our RG impact scenario is robust, then there should be a bias in this correlation function along the direction of radio lobes of the RGs, because more galaxies are formed along the radio-axis triggered by jet/lobe expansion, as compared to directions perpendicular to the radio-jet.

The models investigated in this work and in BW predict the power from the radio lobes only. A natural extension involves the question of whether the same models also fit deeper radio catalogs if we take into account the relativistically Doppler boosted core/jet emission. By incorporating the beamed core emission, investigations of simulations of large scale radio surveys containing many thousands of sources can be done. Some such deep surveys are Faint Images of the Radio Sky at Twenty-cm, FIRST (Becker et al. 1995), the Westerbork Northern Sky Survey, WENSS (Rengelink et al. 1997) and the NRAO VLA Sky Survey, NVSS (Condon et al. 1998), which can be made adequately complete in redshift through optical identifications (Ivezić et al. 2004) from the Sloan Digital Sky Survey, SDSS

(York et al. 2000). If simulations can be performed to predict thousands of sources, the possibility of successfully incorporating a multi-dimensional statistical test becomes much greater.

We thank Christian Kaiser for conversations and clarifying correspondence, Konstantina Manolakou for correspondence and providing us with a version of her Fortran code and Chris Willott for correspondence and for sending us the 6C and 7C-III data. We also benefited from correspondence and conversations with Katherine Blundell, Gopal-Krishna, Zeljko Ivezić and Steve Rawlings. We thank the anonymous referee for several useful suggestions which clarified the presentation of our results. We are most grateful to Angela Osterman for her efforts on initial versions of some codes, PJW is grateful for continuing hospitality at the Department of Astrophysical Sciences at Princeton University. This work was supported in part by a subcontract to GSU from NSF grant AST-0507529 to the University of Washington. PB is supported by the Canada Research Chair program and NSERC.

REFERENCES

Aguirre, A., Schaye, J., Kim, T.-S., Theuns, T., Rauch, M., & Sargent, W. L. W. 2004, *ApJ*, 602, 38

Ajiki, M. et al. 2006, *PASJ*, 58, 499

Barai, P. 2006, PhD Thesis, Georgia State University

Barai, P., & Wiita, P. J. 2006, *MNRAS*, 372, 381 (BW)

Baum, S. A., Zirbel, E. L., & O'Dea, C. P. 1995, *ApJ*, 451, 88

Becker, R. H., White, R. L., & Helfand, D. J. 1995, *ApJ*, 450, 559

Begelman, M. C., & Cioffi, D. F. 1989, *ApJ*, 345, L21

Bîrzan, L., Rafferty, D. A., McNamara, B. R., Wise, M. W., & Nulsen, P. E. J. 2004, *ApJ*, 607, 800

Blundell, K. M., Fabian, A. C., Crawford, C. S., Erlund, M. C., & Celotti, A. 2006, *ApJ*, 644, L13

Blundell, K. M., & Rawlings, S. 1999, *Nature*, 399, 330

Blundell, K. M., Rawlings, S., & Willott, C. J. 1999, *AJ*, 117, 677 (BRW)

Bohringer, H., Nulsen, P. E. J., Braun, R., & Fabian, A. C. 1995, MNRAS, 274, L67

Borderia, M. J. P., Iovino, A., & Bonometto, S. A. 1991, AJ, 102, 495

Bouwens, R., & Illingworth, G. 2006, New Astronomy Review, 50, 152

Cen, R., & Ostriker, J. P. 1999, ApJ, 514, 1

———. 2006, preprint (astro-ph/0601008)

Chambers, K. C., Miley, G. K., & Joyce, R. R. 1988a, ApJ, 329, L75

Chambers, K. C., Miley, G. K., & van Breugel, W. J. M. 1988b, ApJ, 327, L47

Choi, Y.-Y., Reynolds, C. S., Heinz, S., Rosenberg, J. L., Perlman, E. S., & Yang, J. 2004, ApJ, 606, 185

Chokshi, A. 1997, ApJ, 491, 78

Condon, J. J., Cotton, W. D., Greisen, E. W., Yin, Q. F., Perley, R. A., Taylor, G. B., & Broderick, J. J. 1998, AJ, 115, 1693

Davé, R. et al. 2001, ApJ, 552, 473

De Young, D. S. 1989, ApJ, 342, L59

Dey, A., van Breugel, W., Vacca, W. D., & Antonucci, R. 1997, ApJ, 490, 698

Dietrich, M., Hamann, F., Shields, J. C., Constantin, A., Heidt, J., Jäger, K., Vestergaard, M., & Wagner, S. J. 2003, ApJ, 589, 722

Dunlop, J. S., & Peacock, J. A. 1990, MNRAS, 247, 19

Furlanetto, S. R., & Loeb, A. 2001, ApJ, 556, 619

Gopal-Krishna, & Wiita, P. J. 1991, ApJ, 373, 325

———. 2001, ApJ, 560, L115 (GKW01)

———. 2003a, Bull. Astron. Soc. India, 31, 215 (GKW03a)

Gopal-Krishna, & Wiita, P. J. 2003b, in ASP Conf. Ser. 300: Radio Astronomy at the Fringe, ed. J. A. Zensus, M. H. Cohen, & E. Ros (San Francisco: Astronomical Society of the Pacific), 293–300 (GKW03b)

Gopal-Krishna, Wiita, P. J., & Barai, P. 2004, J. Korean Astron. Soc., 37, 517 (GKWB04)

Gopal-Krishna, Wiita, P. J., & Osterman, M. A. 2003, in ASP Conf. Ser. 290: Active Galactic Nuclei: From Central Engine to Host Galaxy, ed. S. Collin, F. Combes, & I. Shlosman (San Francisco: Astronomical Society of the Pacific), 319–322 (GKWO)

Gopal-Krishna, Wiita, P. J., & Saripalli, L. 1989, MNRAS, 239, 173

Greve, T. R., Ivison, R. J., & Stevens, J. A. 2006, Astron. Nachr., 327, 208

Grimes, J. A., Rawlings, S., & Willott, C. J. 2004, MNRAS, 349, 503

Hogg, D. W. 1999, preprint (astro-ph/9905116)

Hopkins, P. F., Richards, G. T., & Hernquist, L. 2006, preprint, submitted to ApJ (astro-ph/0605678)

Ivezić, Ž. et al. 2004, in Multiwavelength AGN Surveys, ed. R. Mújica & R. Maiolino (Singapore: World Scientific Publishing Company), 53–56

Jackson, C. A., & Wall, J. V. 1999, MNRAS, 304, 160

Jeyakumar, S., & Saikia, D. J. 2000, MNRAS, 311, 397 (JS00)

Kaiser, C. R. 2000, A&A, 362, 447 (K2000)

Kaiser, C. R., & Alexander, P. 1997, MNRAS, 286, 215 (KA)

———. 1999, MNRAS, 305, 707

Kaiser, C. R., Dennett-Thorpe, J., & Alexander, P. 1997, MNRAS, 292, 723 (KDA)

Kawakatu, N., & Kino, M. 2006, MNRAS in press (astro-ph/0605482)

Kronberg, P. P., Dufton, Q. W., Li, H., & Colgate, S. A. 2001, ApJ, 560, 178

Laing, R. A., Riley, J. M., & Longair, M. S. 1983, MNRAS, 204, 151

Levine, R., & Gnedin, N. Y. 2005, ApJ, 632, 727

Lilly, S. J., Le Fevre, O., Hammer, F., & Crampton, D. 1996, ApJ, 460, L1

Machalski, J., Chyzy, K. T., & Jamrozy, M. 2004a, Acta Astronomica, 54, 249

———. 2004b, Acta Astronomica, 54, 391

Machalski, J., Chyzy, K. T., Stawarz, L., & Koziel, D. 2006, preprint (astro-ph/0609680)

Madau, P., Pozzetti, L., & Dickinson, M. 1998, *ApJ*, 498, 106

Manolakou, K., & Kirk, J. G. 2002, *A&A*, 391, 127 (MK)

McCarthy, P. J., van Breugel, W. J. M., Spinrad, H., & Djorgovski, S. 1987, *ApJ*, 321, L29

McGilchrist, M. M., Baldwin, J. E., Riley, J. M., Titterington, D. J., Waldram, E. M., & Warner, P. J. 1990, *MNRAS*, 246, 110

O'Dea, C. P., Baum, S. A., Mack, J., Koekemoer, A. M., & Laor, A. 2004, *ApJ*, 612, 131

Overzier, R. A. et al. 2006, *ApJ*, 637, 58

Perucho, M., & Martí, J. M. 2003, *Publications of the Astronomical Society of Australia*, 20, 94

Pieri, M. M., Schaye, J., & Aguirre, A. 2006, *ApJ*, 638, 45

Prochaska, J. X., Weiner, B. J., Chen, H.-W., & Mulchaey, J. S. 2006, *ApJ*, 643, 680

Rawlings, S., Eales, S. A., & Lacy, M. 2001, *MNRAS*, 322, 523

Rawlings, S., & Jarvis, M. J. 2004, *MNRAS*, 355, L9

Rees, M. J. 1989, *MNRAS*, 239, 1P

Rengelink, R. B., Tang, Y., de Bruyn, A. G., Miley, G. K., Bremer, M. N., Röttgering, H. J. A., & Bremer, M. A. R. 1997, *A&AS*, 124, 259

Reynolds, C. S., Brenneman, L. W., & Stocke, J. T. 2005, *MNRAS*, 357, 381

Sawicki, M., & Thompson, D. 2006a, *ApJ*, 642, 653

———. 2006b, *ApJ* in press (astro-ph/0605406)

Schaye, J., Aguirre, A., Kim, T.-S., Theuns, T., Rauch, M., & Sargent, W. L. W. 2003, *ApJ*, 596, 768

Shapley, A. E., Erb, D. K., Pettini, M., Steidel, C. C., & Adelberger, K. L. 2004, *ApJ*, 612, 108

Silk, J. 2005, *MNRAS*, 364, 1337

Spergel, D. N. et al. 2003, *ApJS*, 148, 175

Spergel, D. N. et al. 2006, preprint, submitted to *ApJ* (astro-ph/0603449)

Tripp, T. M., Aracil, B., Bowen, D. V., & Jenkins, E. B. 2006, ApJ, 643, L77

Ueda, Y., Akiyama, M., Ohta, K., & Miyaji, T. 2003, ApJ, 598, 886

Venemans, B. P. et al. 2004, A&A, 424, L17

Venemans, B. P. et al. 2005, A&A, 431, 793

Willott, C. J., Rawlings, S., Blundell, K. M., Lacy, M., & Eales, S. A. 2001, MNRAS, 322, 536

York, D. G. et al. 2000, AJ, 120, 1579

Zheng, W. et al. 2006, ApJ, 640, 574

Table 1. MBRW Model: 1-D KS Statistics for Selected Parameter Variations

x	Model		$\mathcal{P}(P)$	$\mathcal{P}(D)$	$\mathcal{P}(z)$	$\mathcal{P}(\alpha)$	$\mathcal{P}_{[P,D,z,\alpha]}$	$\mathcal{P}_{[P,2D,z,\alpha]}$
T_{Max}^a	Ensemble Size	Survey						
2.6 500	Default ^b 4397469	3C	3.69e-04	5.78e-10	0.00250	6.44e-11	0.404	
		6C	0.202	4.26e-04	0.420	3.58e-10	0.407	
		7C	0.00125	0.00487	0.00317	0.00601		
2.6 250	Default 1466378	3C	8.42e-06	9.61e-08	6.86e-04	2.80e-11	0.451	
		6C	0.0709	0.00193	0.439	9.98e-11	0.578	
		7C	5.11e-05	0.207	8.34e-05	0.00316		
3.0 500	Default 4886474	3C	0.0554	4.87e-06	0.0990	1.11e-15	1.06	
		6C	0.915	0.00708	0.404	3.66e-10	1.12	
		7C	0.00512	0.0883	0.0117	0.00671		
3.0 150	Default 3045199	3C	0.152	0.00101	0.484	4.74e-12	1.29	
		6C	0.434	0.00693	0.574	3.58e-10	1.31	
		7C	1.69e-04	0.0173	2.85e-05	7.21e-04		
3.0 300	Default 4963343	3C	0.177	8.37e-05	0.171	3.29e-13	1.73	
		6C	0.481	0.0402	0.897	3.58e-10	2.23	
		7C	0.00202	0.787	4.54e-04	0.00296		
3.0 300	KDA Env. ^c β, a_0, ρ_0 4963343	3C	0.194	2.37e-08	0.680	0.0632	1.810	
		6C	0.520	7.50e-04	0.956	2.33e-07	1.812	
		7C	7.74e-05	0.00214	4.28e-05	0.0104		
3.0 300	$\beta = 1.0$ 4963343	3C	0.0110	2.76e-10	0.0616	3.54e-08	0.511	
		6C	0.416	1.81e-07	0.183	2.11e-09	0.571	
		7C	6.84e-06	0.0978	2.36e-04	0.00112		
3.0 300	$\beta = 2.0$ 4963343	3C	0.134	1.02e-15	0.358	0.256	0.638 ^g	
		6C	0.0908	7.07e-06	0.335	2.72e-04	0.639 ^g	
		7C	1.60e-04	9.49e-04	1.54e-05	0.0554		

Table 1—Continued

x	Model						$\mathcal{P}_{[P,D,z,\alpha]}$
T_{Max}^a	Ensemble Size	Survey	$\mathcal{P}(P)$	$\mathcal{P}(D)$	$\mathcal{P}(z)$	$\mathcal{P}(\alpha)$	$\mathcal{P}_{[P,2D,z,\alpha]}$
3.0 300	$a_0 = 7.5$ kpc 4963343	3C	0.0530	1.01e-07	0.0532	1.44e-16	0.791
		6C	0.362	0.0626	0.0754	1.96e-06	1.18
		7C	0.0169	0.572	0.00458	0.00861	
3.0 300	$a_0 = 15$ kpc 4963343	3C	0.197	2.25e-04	0.477	3.01e-08	2.07
		6C	0.932	0.00148	0.408	7.24e-09	2.62
		7C	1.32e-04	0.893	3.99e-04	0.00122	
3.0 300	$a_0 = 20$ kpc 4963343	3C	0.0621	1.42e-04	0.112	9.34e-07	0.901
		6C	0.564	0.153	0.408	2.11e-09	1.01
		7C	9.35e-07	0.0247	4.28e-05	5.45e-06	
3.0 300	$\rho_0 = \rho_1^d$ 4963343	3C	0.136	2.50e-06	0.171	1.08e-15	0.790
		6C	0.107	0.0212	0.0126	5.35e-06	1.15
		7C	0.0367	0.565	0.0161	3.15e-05	
3.0 300	$\rho_0 = \rho_2^e$ 4963343	3C	0.0852	4.89e-06	0.387	3.26e-10	1.77
		6C	0.724	0.0582	0.556	2.11e-09	2.26
		7C	2.36e-04	0.741	1.35e-04	1.46e-05	
3.0 300	$\rho_0 = \rho_3^f$ 4963343	3C	0.0229	0.0365	0.0616	3.22e-11	0.656
		6C	0.416	0.0202	0.287	5.79e-13	0.783
		7C	4.48e-07	0.128	2.35e-05	6.46e-07	
3.0 300	$\Gamma_C = 5/3$ 4963343	3C	0.00283	0.00201	0.0105	0.0361	1.13 ^g
		6C	0.987	0.00293	0.764	0.0261	1.14 ^g
		7C	0.698	0.00197	0.569	0.00528	
3.0 300	$\gamma_{min(hs)} = 10$ 4963343	3C	0.253	1.36e-04	0.579	6.02e-11	2.31
		6C	0.831	0.227	0.716	7.62e-08	2.81
		7C	7.70e-05	0.584	1.35e-04	0.00117	

Table 1—Continued

x	Model						$\mathcal{P}_{[P,D,z,\alpha]}$
T_{Max}^a	Ensemble Size	Survey	$\mathcal{P}(P)$	$\mathcal{P}(D)$	$\mathcal{P}(z)$	$\mathcal{P}(\alpha)$	$\mathcal{P}_{[P,2D,z,\alpha]}$
3.0	$\gamma_{max(hs)} = 10^{10}$	3C	0.177	2.79e-05	0.171	3.29e-13	2.29
300	4963343	6C	0.943	0.234	0.994	7.62e-08	3.01
		7C	0.00115	0.932	0.00111	4.56e-04	
3.0	$\gamma_{max(hs)} = 10^{16}$	3C	0.227	8.37e-05	0.220	5.35e-14	1.09
300	4963343	6C	0.533	0.00158	0.272	7.62e-08	1.21
		7C	0.00455	0.199	0.00287	0.00468	
3.0	$p = 2.001$	3C	0.00898	1.59e-05	0.0191	3.98e-16	0.315
300	4963343	6C	0.0661	0.00158	0.00675	2.33e-07	0.490
		7C	0.0353	0.286	0.0344	0.0198	
3.0	$p = 2.5$	3C	0.253	2.36e-04	0.451	1.20e-11	1.79
300	4963343	6C	0.724	0.0361	0.556	7.24e-09	2.06
		7C	2.34e-05	0.412	7.56e-05	0.00534	
3.0	$p = 2.999$	3C	0.198	1.41e-04	0.371	5.09e-12	1.79
300	4963343	6C	0.869	0.0206	0.194	7.24e-09	2.34
		7C	8.02e-05	0.879	1.35e-04	0.00468	
3.0	$t_{bs} = 10^3$ yr	3C	0.130	2.70e-05	0.0532	2.83e-15	0.743
300	4963343	6C	0.509	0.00622	0.109	7.62e-08	0.863
		7C	0.0371	0.190	0.0161	0.0192	
3.0	$t_{bs} = 10^7$ yr	3C	7.23e-04	1.90e-07	6.75e-04	1.28e-07	0.397
300	4963343	6C	0.389	0.0110	0.0667	2.11e-09	0.477
		7C	0.0113	0.121	0.0166	1.46e-05	
3.0	$t_{bf} = 0.01$ yr	3C	0.0978	1.02e-07	0.130	2.79e-15	0.809
300	4963343	6C	0.641	0.00150	0.188	7.62e-08	0.857
		7C	0.00481	0.0770	0.00458	0.00500	

Table 1—Continued

x T_{Max}^a	Model Ensemble Size	Survey	$\mathcal{P}(P)$	$\mathcal{P}(D)$	$\mathcal{P}(z)$	$\mathcal{P}(\alpha)$	$\mathcal{P}_{[P,D,z,\alpha]}$ $\mathcal{P}_{[P,2D,z,\alpha]}$
3.0 300	$t_{bf} = 10$ yr 4963343	3C	0.290	8.81e-06	0.280	2.91e-15	2.06
		6C	0.771	0.0609	0.945	7.62e-08	2.47
		7C	4.03e-04	0.603	6.70e-04	0.00976	
3.0 300	$t_{bf} = 100$ yr 4963343	3C	0.253	8.37e-05	0.622	8.34e-15	2.66
		6C	0.869	0.234	0.862	7.62e-08	3.34
		7C	6.75e-04	0.879	3.99e-04	0.00481	
3.0 300	$t_{bf} = 10^3$ yr 4963343	3C	0.198	2.36e-04	0.579	6.44e-11	2.05
		6C	0.878	0.00300	0.862	7.62e-08	2.23
		7C	3.96e-04	0.286	1.35e-04	0.00500	
3.0 300	$t_{bf} = 100$ yr $\gamma_{min(hs)} = 10$ 4963343	3C	0.113	0.00379	0.483	2.80e-11	2.11
		6C	0.869	0.159	0.716	7.62e-08	2.62
		7C	3.52e-06	0.668	4.28e-05	0.00917	
3.0 300	$t_{bf} = 100$ yr $a_0 = 15$ kpc 4963343	3C	0.0624	2.66e-06	0.247	1.76e-06	1.58
		6C	0.416	0.0992	0.556	2.11e-09	2.23
		7C	0.00115	0.971	7.67e-05	5.49e-04	
3.0 300	$\gamma_{min(hs)} = 10$ $a_0 = 15$ kpc 4963343	3C	0.115	3.97e-07	0.192	3.54e-09	1.17
		6C	0.564	2.50e-05	0.408	7.24e-09	1.42
		7C	6.84e-06	0.412	7.67e-05	3.76e-05	
3.0 300	$t_{bf} = 100$ yr KDA Env. ^c (β, a_0, ρ_0) 4963343	3C	0.147	1.07e-07	0.192	0.0385	1.17
		6C	0.684	0.0626	0.556	6.89e-07	1.22
		7C	3.45e-06	0.0163	1.27e-05	0.0103	

^a T_{Max} in units of Myr.

^bAll other parameters are as in the MBRW model (§2): following Blundell et al. (1999), with hotspot size increasing according to Jeyakumar & Saikia (2000).

^cParameters defining the external environment density profile are set to those of the KDA model: $\beta = 1.9$, $a_0 = 2$ kpc, $\rho_0 = 7.2 \times 10^{-22}$ kg m⁻³.

^d $\rho_1 = \rho_0$ (Default) / 2 = 8.35×10^{-24} kg m⁻³.

^e $\rho_2 = 2 \times \rho_0$ (Default) = 3.34×10^{-23} kg m⁻³.

^f $\rho_3 = 4 \times \rho_0$ (Default) = 6.68×10^{-23} kg m⁻³.

^gNumbers of sources detected in some of the simulated surveys are considerably smaller than in the real surveys, so the 1-D K-S statistic does not hold much significance.

Table 2. MMK Model: 1-D KS Statistics for Selected Parameter Variations

x T_{Max}^a	Model			$\mathcal{P}(P)$	$\mathcal{P}(D)$	$\mathcal{P}(z)$	$\mathcal{P}(\alpha)$	$\mathcal{P}_{[P,D,z,\alpha]}$ $\mathcal{P}_{[P,2D,z,\alpha]}$
	Ensemble Size	Survey						
2.6 500	Default ^b 4397469	3C	0.0931	0.00650	0.124	2.80e-45	0.727 ^c	
		6C	0.105	0.0283	0.575	1.82e-21	0.767 ^c	
		7C	0.0356	0.0309	0.130	7.92e-22		
2.6 150	Default 3888492	3C	0.0491	0.521	0.535	0	2.12	
		6C	0.624	0.102	0.506	1.83e-24	2.88	
		7C	0.00187	0.301	0.0491	6.13e-21		
2.6 250	Default 4195764	3C	9.76e-04	0.216	0.421	0	1.64	
		6C	0.0935	3.44e-04	0.681	1.83e-24	2.36	
		7C	2.38e-05	0.827	0.0115	4.30e-20		
2.6 300	Default 4342468	3C	0.00152	0.0125	0.421	0	1.72	
		6C	0.641	0.252	0.0709	1.83e-24	2.34	
		7C	0.0105	0.732	0.235	6.13e-21		
3.0 150	Default 4861474	3C	1.21e-07	0.0366	1.47e-08	0	0.558	
		6C	0.212	0.371	0.0265	2.99e-26	0.911	
		7C	0.00341	0.134	0.0541	7.92e-22		
3.0 500	Default 4886474	3C	2.30e-04	0.195	6.52e-05	1.58e-31	0.410 ^c	
		6C	0.154	0.0125	0.00722	8.88e-16	0.611 ^c	
		7C	0.145	0.128	0.0532	6.13e-21		
2.6 150	KDA Env. ^d β, a_0, ρ_0 3888492	3C	0.00553	0.00253	0.485	0	1.55	
		6C	0.157	0.485	0.556	1.83e-24	2.15	
		7C	1.24e-05	0.483	0.00180	2.79e-19		
2.6 150	$\beta = 1.0$ 3888492	3C	0.00368	8.37e-05	0.474	0	1.27	
		6C	0.331	7.50e-04	0.498	1.83e-24	1.54	
		7C	4.26e-05	0.434	0.00710	8.39e-22		

Table 2—Continued

x T_{Max}^a	Model Ensemble Size	Survey	$\mathcal{P}(P)$	$\mathcal{P}(D)$	$\mathcal{P}(z)$	$\mathcal{P}(\alpha)$	$\mathcal{P}_{[P,D,z,\alpha]}$ $\mathcal{P}_{[P,2D,z,\alpha]}$
2.6 150	$\beta = 1.6$ 3888492	3C	0.121	0.709	0.535	0	2.73
		6C	0.724	0.103	0.408	1.83e-24	4.04
		7C	0.00479	0.879	0.0491	4.15e-20	
2.6 150	$a_0 = 7.5$ kpc 3888492	3C	0.0913	0.615	0.360	0	1.98
		6C	0.707	0.102	0.125	1.83e-24	2.91
		7C	0.00703	0.412	0.0689	6.13e-21	
2.6 150	$a_0 = 20$ kpc 3888492	3C	0.0253	0.802	0.192	0	2.28
		6C	0.564	0.0212	0.533	1.83e-24	3.64
		7C	1.34e-04	0.893	0.00708	8.39e-22	
2.6 150	$\rho_0 = \rho_1^e$ 3888492	3C	0.0921	0.0260	0.0399	0	0.987
		6C	0.229	0.0117	0.655	1.83e-24	1.27
		7C	6.56e-04	0.412	0.0108	4.30e-20	
2.6 150	$\rho_0 = \rho_2^f$ 3888492	3C	0.00826	0.425	0.483	0	1.58
		6C	0.293	7.50e-04	0.556	1.83e-24	2.13
		7C	7.74e-05	0.204	0.00291	6.13e-21	
2.6 150	$\gamma_{min(hs)} = 7$ 3888492	3C	0.0921	0.0697	0.101	0	1.31
		6C	0.224	0.102	0.556	1.83e-24	1.93
		7C	2.33e-05	0.790	0.0108	8.39e-22	
2.6 150	$\gamma_{min(hs)} = 100$ 3888492	3C	8.29e-04	2.01e-07	0.00485	0	0.199
		6C	0.0809	4.05e-06	0.199	6.76e-22	0.216
		7C	9.50e-10	0.0267	9.25e-07	1.74e-18	
2.6 150	$\gamma_{max(hs)} = 3 \times 10^8$ 3888492	3C	0.0674	0.212	0.360	0	1.69
		6C	0.869	0.159	0.503	1.83e-24	2.03
		7C	0.00307	0.0465	0.0491	6.13e-21	

Table 2—Continued

x	Model						$\mathcal{P}_{[P,D,z,\alpha]}$
T_{Max}^a	Ensemble Size	Survey	$\mathcal{P}(P)$	$\mathcal{P}(D)$	$\mathcal{P}(z)$	$\mathcal{P}(\alpha)$	$\mathcal{P}_{[P,2D,z,\alpha]}$
2.6 150	$p = 2.001$ 3888492	3C	0.0629	0.00159	0.483	2.45e-39	1.22
		6C	0.575	2.55e-05	0.362	4.45e-21	1.31
		7C	1.36e-04	0.131	0.00458	6.90e-17	
2.6 150	$p = 2.3$ 3888492	3C	0.0356	0.510	0.135	0	2.02
		6C	0.293	0.102	0.716	1.83e-24	3.20
		7C	0.00108	0.999	0.0238	3.72e-20	
2.6 150	$\epsilon = 0.675$ 3888492	3C	0.0911	0.00159	0.227	0	1.07
		6C	0.564	0.00158	0.408	1.83e-24	1.19
		7C	6.64e-04	0.190	0.0161	6.13e-21	
2.6 150	$\epsilon = 1.4$ 3888492	3C	0.122	0.619	0.568	0	2.22
		6C	0.479	0.349	0.408	1.35e-23	3.18
		7C	2.44e-04	0.199	0.0108	4.30e-20	
2.6 150	$\eta = 0.2$ 3888492	3C	0.00922	0.0365	7.11e-04	0	1.01 ^c
		6C	0.333	7.50e-04	0.533	1.83e-24	1.17 ^c
		7C	0.0173	0.204	0.293	4.30e-20	
2.6 150	$\eta = 0.6$ 3888492	3C	0.0175	0.532	0.192	0	1.44
		6C	0.416	0.00152	0.556	1.83e-24	2.05
		7C	1.10e-07	0.128	6.81e-04	4.15e-20	
2.6 150	$\tau = 2 \times 10^{-4}$ 3888492	3C	0.0253	4.88e-05	0.112	0	0.680
		6C	0.564	1.65e-07	0.267	1.40e-23	0.696
		7C	3.58e-06	0.0273	4.06e-04	1.74e-18	
2.6 150	$\tau = 3 \times 10^{-3}$ 3888492	3C	0.0497	0.167	0.135	0	1.37
		6C	0.0959	0.240	0.564	1.83e-24	2.14
		7C	1.34e-04	0.732	0.00708	5.91e-21	

Table 2—Continued

x	Model						$\mathcal{P}_{[P,D,z,\alpha]}$
T_{Max}^a	Ensemble Size	Survey	$\mathcal{P}(P)$	$\mathcal{P}(D)$	$\mathcal{P}(z)$	$\mathcal{P}(\alpha)$	$\mathcal{P}_{[P,2D,z,\alpha]}$
2.6	$\epsilon = 1.4$	3C	0.0906	0.178	0.580	0	1.98
150	$\beta = 1.6$	6C	0.416	0.242	0.408	1.40e-23	2.76
	3888492	7C	0.00110	0.732	0.0108	2.79e-19	
2.6	$\epsilon = 1.4$	3C	0.0910	0.216	0.581	0	2.04
150	$a_0 = 7.5$ kpc	6C	0.340	0.485	0.408	1.40e-23	2.90
	3888492	7C	0.00108	0.565	0.0238	1.74e-18	
2.6	$\beta = 1.6$	3C	0.207	0.216	0.535	0	2.26
150	$a_0 = 7.5$ kpc	6C	0.724	0.340	0.194	1.35e-23	3.13
	3888492	7C	0.0106	0.732	0.0491	4.30e-20	

^a T_{Max} in units of Myr.

^bAll other parameters are as in the MMK model (§2): following Manolakou & Kirk (2002), with hotspot size increasing according to Jeyakumar & Saikia (2000).

^cOne cannot be confident of the validity of the K-S statistic as the detected sample in the simulation is smaller (or, much smaller) than in the actual catalog.

^dParameters defining the external environment density profile are set to those of the KDA model: $\beta = 1.9$, $a_0 = 2$ kpc, $\rho_0 = 7.2 \times 10^{-22}$ kg m⁻³.

^e $\rho_1 = \rho_0$ (Default) / 1.5 = 1.133×10^{-23} kg m⁻³.

^f $\rho_2 = 2 \times \rho_0$ (Default) = 3.4×10^{-23} kg m⁻³.

Table 3. K2000 Model: 1-D K-S Statistics for a Few Parameter Variations

x T_{Max} ^a	Model		$\mathcal{P}(P)$	$\mathcal{P}(D)$	$\mathcal{P}(z)$	$\mathcal{P}(\alpha)$	$\mathcal{P}_{[P,D,z,\alpha]}$
	Ensemble Size	Survey					$\mathcal{P}_{[P,2D,z,\alpha]}$
2.6 500	Default ^b 114900	3C	5.95e-11	4.06e-12	8.21e-07	3.89e-42	0.0127
		6C	0.00110	3.59e-09	0.0185	1.80e-24	0.0130
		7C	9.89e-17	5.39e-04	1.24e-09	1.91e-13	
3.0 150	Default 4861474	3C	8.30e-09	0.0151	2.69e-07	3.89e-42	0.152
		6C	3.05e-06	2.13e-04	0.00264	1.80e-24	0.302
		7C	1.04e-19	0.221	1.48e-13	1.91e-13	
3.0 150	Default 111072	3C	8.30e-09	0.0200	3.53e-06	2.00e-41	0.241
		6C	8.19e-05	1.52e-04	0.00211	4.92e-21	0.481
		7C	4.28e-21	0.360	9.20e-14	2.78e-13	

^a T_{Max} in units of Myr.

^bAll other dynamical and lobe power evolution model parameters are same as in the fiducial model of K2000 (Kaiser 2000).

Table 4. Model 1-D K-S Statistics using Grimes, Rawlings, & Willott (2004) RLF

x T_{Max}^b	Model ^a Ensemble Size	Survey	$\mathcal{P}(P)$	$\mathcal{P}(D)$	$\mathcal{P}(z)$	$\mathcal{P}(\alpha)$	$\frac{\mathcal{P}_{[P,D,z,\alpha]}}{\mathcal{P}_{[P,2D,z,\alpha]}}$
2.6 500	KDA 3712083	3C	5.59e-08	8.84e-06	1.01e-04	3.01e-08	0.494
		6C	0.140	0.00193	0.310	3.66e-10	0.690
		7C	0.0122	0.319	0.00202	0.0106	
3.0 100	KDA 1958652	3C	0.0281	0.0976	0.0583	3.34e-09	0.410
		6C	0.107	0.0204	0.0397	1.96e-06	0.633
		7C	0.00303	0.120	0.00699	0.00230	
3.0 150	KDA 2747159	3C	0.0611	0.217	0.0836	1.28e-11	1.14
		6C	0.394	0.349	0.0735	6.89e-07	1.82
		7C	0.0173	0.264	0.0114	3.26e-05	
3.0 200	KDA 3212793	3C	0.133	0.0125	0.180	1.36e-10	1.44
		6C	0.416	0.00615	0.191	6.89e-07	2.14
		7C	0.0362	0.732	0.00728	0.0198	
3.0 300	KDA 3813260	3C	0.175	0.0253	0.387	5.04e-14	1.39
		6C	0.115	0.349	0.0245	6.89e-07	2.12
		7C	0.00728	0.524	0.00464	0.00500	
3.0 500	KDA 5105485	3C	0.122	0.00101	0.192	1.41e-09	1.32
		6C	0.0454	0.0968	0.0255	1.96e-06	2.26
		7C	0.00466	0.942	0.0165	0.00468	
2.6 500	BRW 3712083	3C	4.63e-07	5.54e-08	3.43e-05	8.34e-04	0.467
		6C	0.0770	0.0265	0.212	3.66e-10	0.751
		7C	5.04e-05	0.438	9.03e-05	0.00304	
3.0 100	BRW 1958652	3C	5.84e-06	2.27e-21	2.04e-05	0.00483	0.303
		6C	0.177	0.00158	0.194	6.76e-07	0.363
		7C	6.84e-06	0.0643	1.27e-05	0.0104	

Table 4—Continued

x	Model ^a							$\mathcal{P}_{[P,D,z,\alpha]}$
T_{Max} ^b	Ensemble Size	Survey	$\mathcal{P}(P)$	$\mathcal{P}(D)$	$\mathcal{P}(z)$	$\mathcal{P}(\alpha)$	$\mathcal{P}_{[P,2D,z,\alpha]}$	
3.0 150	BRW 2747159	3C	3.63e-05	5.73e-19	6.18e-05	0.0328	0.629	
		6C	0.129	0.00158	0.287	2.33e-07	0.959	
		7C	6.67e-04	0.353	1.36e-04	0.0104		
3.0 200	BRW 3212793	3C	5.69e-05	5.00e-18	5.93e-05	0.0264	0.828	
		6C	0.177	0.00622	0.287	1.89e-06	1.33	
		7C	2.29e-04	0.533	3.99e-04	0.0194		
3.0 300	BRW 3813260	3C	2.91e-04	3.53e-16	1.05e-04	0.0857	0.769	
		6C	0.113	7.50e-04	0.287	6.76e-07	1.17	
		7C	0.0159	0.434	0.00180	0.0198		
3.0 500	BRW 5105485	3C	3.00e-04	2.00e-21	2.94e-04	4.23e-04	0.694	
		6C	0.293	6.60e-05	0.287	2.33e-07	1.02	
		7C	7.74e-05	0.353	7.67e-05	0.00500		
2.6 500	MK 3712083	3C	5.82e-11	1.27e-09	1.95e-05	0	0.712	
		6C	0.161	0.00203	0.432	1.80e-24	1.05	
		7C	1.55e-05	0.548	0.00126	1.58e-15		
3.0 100	MK 1958652	3C	0.0122	0.0187	0.148	0	0.674	
		6C	0.564	0.156	0.0142	1.40e-23	0.819	
		7C	0.00747	0.0323	0.00189	2.09e-15		
3.0 150	MK 2747159	3C	0.0494	0.125	0.458	0	1.36	
		6C	0.396	0.336	0.0142	1.40e-23	1.95	
		7C	0.00181	0.278	0.00484	2.16e-15		
3.0 200	MK 3212793	3C	0.00557	0.0253	0.222	0	1.26	
		6C	0.798	0.323	0.0735	1.02e-22	1.73	
		7C	0.00185	0.272	0.00471	2.09e-15		

Table 4—Continued

x	Model ^a		Survey	$\mathcal{P}(P)$	$\mathcal{P}(D)$	$\mathcal{P}(z)$	$\mathcal{P}(\alpha)$	$\mathcal{P}_{[P,D,z,\alpha]}$
T_{Max} ^b	Ensemble Size	$\mathcal{P}_{[P,2D,z,\alpha]}$						
3.0	MK	3C	0.0250	0.00247	0.247	0	1.11	
		6C	0.498	0.159	0.0136	9.89e-23	1.61	
		7C	0.0255	0.422	0.00479	2.03e-15		
3.0	MK	3C	0.00366	0.0259	0.474	0	0.897	
		6C	0.0441	0.0200	1.69e-04	9.89e-23	1.24	
		7C	0.0484	0.327	0.00471	3.94e-16		
2.6	MBRW	3C	9.04e-05	8.84e-06	0.00288	1.52e-08	0.50524	
		6C	0.564	2.55e-05	0.189	7.62e-08	0.50527	
		7C	0.0170	5.25e-06	0.00703	0.0194		
3.0	MBRW	3C	0.0443	0.0186	0.0320	3.26e-10	0.435	
		6C	0.278	0.0984	0.118	7.62e-08	0.543	
		7C	0.00486	0.0300	6.70e-04	1.41e-05		
3.0	MBRW	3C	0.152	0.00159	0.0616	1.95e-14	0.619	
		6C	0.118	0.102	0.0255	7.62e-08	0.930	
		7C	0.00307	0.264	0.00291	3.32e-05		
3.0	MBRW	3C	0.194	4.87e-06	0.192	1.28e-13	0.938	
		6C	0.727	0.0103	0.118	7.62e-08	0.950	
		7C	0.00450	0.00595	0.0107	9.01e-05		
3.0	MBRW	3C	0.253	0.00159	0.192	5.09e-12	0.707	
		6C	0.276	0.0117	0.0735	7.62e-08	0.734	
		7C	0.00481	0.0194	0.0111	0.00500		
3.0	MBRW	3C	0.385	1.42e-06	0.312	9.59e-07	0.882	
		6C	0.120	0.00150	0.0255	7.62e-08	0.923	
		7C	0.0358	0.0430	0.0160	0.00976		

Table 4—Continued

x	Model ^a		Survey	$\mathcal{P}(P)$	$\mathcal{P}(D)$	$\mathcal{P}(z)$	$\mathcal{P}(\alpha)$	$\mathcal{P}_{[P,D,z,\alpha]}$
T_{Max} ^b	Ensemble Size							$\mathcal{P}_{[P,2D,z,\alpha]}$
2.6	MMK	3C	0.0681	0.0125	0.474	0	1.15	
		6C	0.724	0.00300	0.177	1.83e-24	1.20	
		7C	0.00451	0.0294	0.00710	4.15e-20		
3.0	MMK	3C	0.0200	0.00851	0.00903	0	0.210	
		6C	0.107	0.154	0.00189	1.83e-24	0.316	
		7C	0.00750	0.00102	0.00114	4.00e-20		
3.0	MMK	3C	0.103	0.0696	0.0206	0	0.219	
		6C	0.00775	1.44e-04	1.19e-05	1.83e-24	0.298	
		7C	0.0115	0.00920	0.00188	5.91e-21		

^aAll the dynamical and radio lobe power evolution model parameters are same as in the default version of the corresponding model (KDA, BRW, MK, MBRW, MMK).

^b T_{Max} in units of Myr.

Table 5. 2-D K-S Test Results for the Two Modified Models

Model Parameters	Survey	2-D KS Probability, $\mathcal{P}(\text{K-S})$					
		$\mathcal{P}(P-z)$	$\mathcal{P}(P-D)$	$\mathcal{P}(z-D)$	$\mathcal{P}(P-\alpha)$	$\mathcal{P}(z-\alpha)$	$\mathcal{P}(D-\alpha)$
MBRW	3C	0.00234	4.17e-10	2.10e-08	8.27e-08	6.07e-08	5.47e-12
Default ^a	6C	0.458	0.00506	0.00667	1.46e-06	1.48e-06	1.53e-04
	7C	0.00309	8.54e-04	0.00222	0.00733	0.00648	0.0112
MBRW	3C	0.299	0.00119	0.00246	5.99e-11	3.86e-10	4.64e-14
Varied ^b	6C	0.781	0.434	0.496	3.21e-06	7.85e-06	2.76e-04
	7C	1.60e-04	0.00297	0.00237	6.00e-05	6.28e-05	0.00228
MMK	3C	0.0366	1.48e-04	0.00444	2.29e-40	2.28e-39	1.88e-32
Default ^c	6C	0.0656	0.0325	0.183	1.70e-17	2.32e-18	3.76e-16
	7C	0.0151	0.00180	0.00355	3.53e-15	5.25e-14	2.88e-13
MMK	3C	0.147	0.143	0.421	8.35e-40	5.53e-37	8.64e-30
Varied ^d	6C	0.254	0.282	0.235	1.53e-17	2.08e-18	2.22e-14
	7C	0.0203	0.00627	0.0290	2.27e-14	2.96e-13	2.91e-12

^aSimulations with the respective parameters of MBRW model as used in §2. Initial population generated using $x = 2.6$, $T_{Max} = 500$ Myr.

^bMBRW model simulation using initial population with $x = 3.0$, $T_{Max} = 300$ Myr. The power evolution is with parameter change $t_{bf} = 100$ yr, other parameters set to their default values, for a case with initial source population size = 4963343 (the last but 6th entry in Table 1).

^cSimulations with the respective parameters of MMK model as used in §2. Initial population generated using $x = 2.6$, $T_{Max} = 500$ Myr.

^dMMK model simulation using initial population with $x = 2.6$, $T_{Max} = 150$ Myr. The power evolution is with parameter change $\beta = 1.6$, other parameters set to their default values, for a case with initial source population size = 3888492 (9th entry in Table 2).

Table 6. 4-variable Spearman Partial Rank Correlation Analysis ^a

Coeff.	All ^a	Model (combining all surveys ^a)			
		MBRW		MMK	
		Default	Varied ^b	Default	Varied ^b
$r_{PD,z\alpha}$ ^c	0.0303	0.183	0.0309	0.160	0.127
$\Sigma_{PD,z\alpha}$ ^d	0.478	2.94	0.489	2.57	2.02
$r_{Pz,D\alpha}$	0.716	0.667	0.649	0.0754	-0.103
$\Sigma_{Pz,D\alpha}$	14.2	12.8	12.2	1.20	-1.64
$r_{Dz,P\alpha}$	-0.268	-0.348	-0.237	0.218	0.00189
$\Sigma_{Dz,P\alpha}$	-4.33	-5.77	-3.83	3.52	0.0300
$r_{P\alpha,Dz}$	0.147	-0.0163	-0.0139	-0.640	-0.750
$\Sigma_{P\alpha,Dz}$	2.33	-0.259	-0.219	-12.1	-15.4
$r_{D\alpha,Pz}$	0.472	0.0649	-0.275	0.605	0.346
$\Sigma_{D\alpha,Pz}$	8.08	1.03	-4.47	11.2	5.72
$r_{z\alpha,PD}$	-0.0234	0.132	0.194	-0.590	-0.609
$\Sigma_{z\alpha,PD}$	-0.369	2.12	3.12	-10.8	-11.2

^aThe four observables P , D , z and α for the 3C, 6C and 7C III surveys (whether real or simulated), combined together in a single sample.

^bThe particular parameters used are the same as those in Table 5 for each of the MBRW and MMK *varied* models.

^cSpearman partial rank correlation coefficient between two variables P and D , when the other two variables z and α are kept fixed.

^dSignificance level associated with the correlation between P and D , independent of z and α .

Table 7. Relevant Volume Fractions for Selected Models and Modifications

x	T_{Max} (Myr)	Ensemble Size	Model Parameters	Ratio _{3C}	A_z ($\times 10^{-8}$) (Mpc $^{-3}$)	Volume Fraction, ι	Total Vol-Frac, ζ
BRW model							
2.6	250	1466378	Default	2.12	0.931	0.00147	0.00623
2.6	500	1561417	Default	1.15	0.532	0.0123	0.0301
3.0	250	1571349	Default	1.33	0.997	0.00204	0.00863
3.0	250	3355926	$a_0 = 7.5$ kpc ^a	0.869	2.13	0.00964	0.0408
3.0	500	2930490	Default	1.21	0.997	0.0179	0.0437
3.0	500	6451283	$a_0 = 7.5$ kpc	1.03	2.19	0.0667	0.163
MBRW model							
2.6	500	4397469	Default	2.87	1.50	0.0139	0.0339
3.0	300	4963343	$t_{bf} = 100$ yr ^b	1.94	2.66	0.00658	0.0240
KDA model							
2.6	150	1553389	Default	2.17	1.60	0.000324	0.00215
2.6	500	4397469	Default	2.18	1.50	0.0183	0.0452
3.0	150	1618248	Default	0.703	1.66	0.000796	0.00530
3.0	150	4861474	p, ρ_0 ^{c,d}	0.993	4.99	0.00331	0.0220
3.0	500	3419466	Default	0.559	1.16	0.0428	0.106
3.0	500	6451283	p, ρ_0 ^c	0.393	2.19	0.225	0.555
MK model							
2.6	150	3888492	Default	3.26	3.99	0.000772	0.00512
2.6	500	4397469	Default	1.37	1.50	0.0286	0.0699
3.0	150	4861474	Default	1.20	4.99	0.00213	0.0141
3.0	150	4861474	$\gamma_{max(hs)}$ ^{e,f}	1.11	4.99	0.00230	0.0153
3.0	500	4886474	Default	0.421	1.66	0.0844	0.206
3.0	500	4886474	$\gamma_{max(hs)}$ ^e	0.414	1.66	0.0858	0.209
MMK model							
2.6	150	3888492	$\beta = 1.6$ ^g	1.59	3.99	0.00220	0.0146

Table 7—Continued

x	T_{Max} (Myr)	Ensemble Size	Model Parameters	Ratio _{3C}	A_z ($\times 10^{-8}$) (Mpc $^{-3}$)	Volume Fraction, ι	Total Vol-Frac, ζ
2.6	500	4397469	Default	0.710	1.50	0.0552	0.135

^a1-D K-S best-fit case of BRW.

^b1-D K-S best-fit case of MBRW.

^cParameter variations: $p = 2.12$ and $\rho_0 = \rho_0$ (Default)/2 = 3.6×10^{-22} kg m $^{-3}$.

^d1-D K-S best-fit case of KDA.

^eParameter variation: $\gamma_{max(hs)} = 3 \times 10^8$.

^f1-D K-S best-fit case of MK.

^g1-D K-S best-fit case of MMK.